Behavioral/Cognitive

Interaural Place-of-Stimulation Mismatch Estimates Using CT Scans and Binaural Perception, But Not Pitch, Are Consistent in Cochlear-Implant Users

Joshua G.W. Bernstein,[1] Kenneth K. Jensen,[1] Olga A. Stakhovskaya,[2] Jack H. Noble,[3] Michael Hoa,[4] H. Jeffery Kim,[4] Robert Shih,[5] Elizabeth Kolberg,[2] Miranda Cleary,[2] and Matthew J. Goupell[2]

[1]National Military Audiology and Speech Pathology Center, Walter Reed National Military Medical Center, Bethesda, Maryland 20889, [2]Department of Hearing and Speech Sciences, University of Maryland, College Park, Maryland 20742, [3]Department of Electrical Engineering and Computer Science, Vanderbilt University, Nashville, Tennessee 37232, [4]Department of Otolaryngology Head and Neck Surgery, Georgetown University Medical Center, Washington, DC 20057, and [5]Department of Radiology, Walter Reed National Military Medical Center, Bethesda, Maryland 20889

Bilateral cochlear implants (BI-CIs) or a CI for single-sided deafness (SSD-CI; one normally functioning acoustic ear) can partially restore spatial-hearing abilities, including sound localization and speech understanding in noise. For these populations, however, interaural place-of-stimulation mismatch can occur and thus diminish binaural sensitivity that relies on interaurally frequency-matched neurons. This study examined whether plasticity—reorganization of central neural pathways over time—can compensate for peripheral interaural place mismatch. We hypothesized differential plasticity across two systems: none for binaural processing but adaptation for pitch perception toward frequencies delivered by the specific electrodes. Interaural place mismatch was evaluated in 19 BI-CI and 23 SSD-CI human subjects (both sexes) using binaural processing (interaural-time-difference discrimination with simultaneous bilateral stimulation), pitch perception (pitch ranking for single electrodes or acoustic tones with sequential bilateral stimulation), and physical electrode-location estimates from computed-tomography (CT) scans. On average, CT scans revealed relatively little BI-CI interaural place mismatch (26° insertion-angle mismatch) but a relatively large SSD-CI mismatch, particularly at low frequencies (166° for an electrode tuned to 300 Hz, decreasing to 14° at 7000 Hz). For BI-CI subjects, the three metrics were in agreement because there was little mismatch. For SSD-CI subjects, binaural and CT measurements were in agreement, suggesting little binaural-system plasticity induced by mismatch. The pitch measurements disagreed with binaural and CT measurements, suggesting place-pitch plasticity or a procedural bias. These results suggest that reducing interaural place mismatch and potentially improving binaural processing by reprogramming the CI frequency allocation would be better done using CT-scan than pitch information.

Key words: binaural; brainstem; interaural time difference; mismatch; plasticity; superior olivary complex

Significance Statement

Electrode-array placement for cochlear implants (bionic prostheses that partially restore hearing) does not explicitly align neural representations of frequency information. The resulting interaural place-of-stimulation mismatch can diminish spatial-hearing abilities. In this study, adults with two cochlear implants showed reasonable interaural alignment, whereas those with one cochlear implant but normal hearing in the other ear often showed mismatch. In cases of mismatch, binaural sensitivity was best when the same cochlear locations were stimulated in both ears, suggesting that binaural brainstem pathways do not experience plasticity to compensate for mismatch. In contrast, interaurally pitch-matched electrodes deviated from cochlear-location estimates and did not optimize binaural sensitivity. Clinical correction of interaural place mismatch using binaural or computed-tomography (but not pitch) information may improve spatial-hearing benefits.

Introduction

The superior olivary complex (SOC; Yin et al., 2019) of the brainstem provides exquisite interaural-time-difference (ITD) and interaural-level-difference (ILD) sensitivity, facilitating sound-source localization and speech understanding in noise (Reeder et al., 2014). To partially restore these advantages to those with hearing impairment, there is a growing population of cochlear-implant (CI) users with two functional ears: bilateral CIs (BI-CIs; both ears) for bilateral hearing loss (Peters et al., 2010) or one CI for single-sided deafness (SSD-CI; normal/near-normal hearing in the unimplanted ear; Buss et al., 2018).

Under laboratory-controlled conditions, many human BI-CI and SSD-CI users demonstrate behavioral ITD sensitivity (Kan and Litovsky, 2015; Bernstein et al., 2018). Cat and rabbit inferior colliculus neurons also show electrical stimulation ITD sensitivity (Hancock et al., 2013; Chung et al., 2016). Although BI-CI and SSD-CI users experience some two-ear advantages with everyday sound processors (Litovsky et al., 2012; Bernstein et al., 2016, 2017), these are diminished compared with normal-hearing individuals. Various factors might limit binaural benefits, including lack of temporal-fine-structure encoding (Churchill et al., 2014) or CI versus acoustic ear time delays (Zirn et al., 2015).

The limiting factor examined here was across-ear frequency misalignment. In normal-hearing systems, peripheral tonotopy reflects physical cochlear dimensions (Greenwood, 1990) that are typically symmetric (Reda et al., 2014), and SOC neurons receive frequency-matched binaural inputs (Blanks et al., 2007). In contrast, typical CI frequency-to-electrode allocation prioritizes the full speech spectrum, ignoring physical electrode locations that determine cochlear place of stimulation. This can result in interaural place-of-stimulation differences for BI-CI (mismatched array placement) or SSD-CI (mismatch between electrode location and acoustic tonotopy; Landsberger et al., 2015) users. Mismatch can reduce binaural sensitivity (Poon et al., 2009), localization performance (Suneel et al., 2017), and speech understanding in the presence of competing talkers (Wess et al., 2017). However, a critical question remains unanswered; that is, can binaural neurons adapt to respond to input from different cochlear locations?

CI users show evidence of plasticity to frequency-to-place mismatch for monaural speech understanding (Svirsky et al., 2004) and for interaural place-pitch comparisons (Reiss et al., 2014), but neither requires brainstem processing of simultaneous binaural stimuli. Although there is evidence for remapping of binaural cues to physical sound-source locations (Van Wanrooij and Van Opstal, 2005), this might only require cortical plasticity to reinterpret brainstem outputs. Hu and Dietz (2015) suggested

little binaural plasticity to interaural place mismatch. They compared BI-CI binaural (specifically ITD) processing for simultaneous bilateral single-electrode stimulation (using perceptual and electrophysiological methods) to pitch perception for sequential bilateral stimulation (one ear then the other). Pitch-matched bilateral electrode pairs were usually number-matched, but pairs yielding the best binaural performance were not. This was interpreted as evidence for plasticity for place-pitch perception but not binaural processing, although the evidence was indirect because physical electrode locations were unknown. Other studies compared SSD-CI pitch matching and computed-tomography (CT) scans (Schatzer et al., 2014; Adel et al., 2019) but did not assess binaural processing. The three methods have never been compared in the same subjects.

To investigate interaural-place-mismatch plasticity, we compared ITD matches (Which electrode or acoustic frequency produces the best binaural sensitivity for a given electrode in the other ear?), place-pitch matches (Which produces an equivalent pitch percept?), and CT-scan matches (Which has the same physical location?). Because binaural sensitivity typically relies on frequency-matched inputs to the brainstem—a relatively low-level system—we hypothesized that plasticity would not be evident, with ITD-based estimates aligning with CT-based electrode location estimates. In contrast, sequential place-pitch comparisons do not require binaural brainstem processing. Because cortical tonotopic maps can shift following peripheral changes (Robertson and Irvine, 1989), we hypothesized that plasticity would be evident (Reiss et al., 2007), with pitch-based estimates aligning with an electrode's frequency allocation in the subject's clinical sound processor. We also hypothesized more mismatch for SSD-CI users because mismatch between the electrode array and cochlear tonotopy is common, with electrodes rarely reaching the cochlear apex (Canfarotta et al., 2020), than for BI-CI users who only have relative mismatch in insertion depths.

Materials and Methods

Subjects

A total of 42 subjects (19 BI-CI and 23 SSD-CI) participated in the study (Tables 1, 2). These subjects had a wide range of ages, duration of deafness, and etiology, but all subjects had used their CIs for at least 6 months at the time of the study. The BI-CI subjects were all implanted in both ears with Cochlear-brand devices; 16 subjects had precurved arrays in both ears, and 3 subjects had a straight array in one ear and a precurved array in the other ear. The SSD-CI subjects were implanted with a Cochlear-brand or MED-EL device in one ear; 7 subjects were implanted with a precurved array and 16 subjects with a straight array. The other ear had either normal hearing thresholds [$N = 16$; $\leq$25 dB hearing level (HL) for octave frequencies between 250 and 4000 Hz] or mild ($N = 5$; $\leq$40 dB HL) or moderate hearing loss ($N = 2$; $\leq$60 dB HL). Four subjects with mild or moderate hearing loss usually wore a hearing

Table 1. Demographic and device information for the BI-CI subjects

| Subject | Age | Sex | Left ear | | | | Right ear | | | |
			Duration of deafness (years)	CI experience (years)	Array model	Array type	Duration of deafness (years)	CI experience (years)	Array model	Array type
BCI1	72	F	36	22	CI24M	S	44	15	CI24R(CS)	P
BCI2	78	M	3	16	CI24R(CS)	P	7	10	CI24RE	P
BCI3	66	F	2	11	CI24RE	P	1	12	CI24RE	P
BCI4	71	F	<1	18	CI24R(CS)	P	4	13	CI24RE	P
BCI5	67	F	5	12	CI24RE	P	7	15	CI24R(CA)	P
BCI6	71	M	>20	3	CI422	S	<1	15	CI24R(CS)	P
BCI7	59	F	11	8	CI24RE	P	11	8	CI24RE	P
BCI8	65	F	12	8	CI512	P	13	7	CI24RE	P
BCI9	78	M	61	5	CI24RE	P	1	8	CI512	P
BCI10	52	F	<1	9	CI512	P	2	3	CI512	P
BCI11	72	F	13	10	CI24RE	P	<1	13	CI24RE	P
BCI12	69	F	<1	10	CI24RE	P	<1	8	CI512	P
BCI13	70	F	1	8	CI24RE	P	2	7	CI512	P
BCI14	67	M	14	6	CI24RE	P	23	5	CI24RE	P
BCI15	69	F	9	9	CI512	P	9	9	CI512	P
BCI16	50	F	24	4	CI422	S	20	8	CI24RE	P
BCI17	76	F	27	9	CI24RE	P	29	7	CI512	P
BCI18	48	M	<1	2	CI532	P	6	4	CI24RE	P
BCI19	25	M	<1	7	CI24RE	P	<1	7	CI24RE	P

P, Precurved; S, straight.

Table 2. Demographic and device information for the SSD-CI subjects

Subject	Age	Sex	CI ear	Duration of deafness (years)	CI experience (years)	Array model	Array type	Acoustic ear
SSD1	60	M	R	8	2	Flex28	S	Mild SNHL
SSD2	36	M	R	<1	5	Flex28	S	NH
SSD3	46	M	R	22	5	Flex28	S	NH
SSD4	63	F	L	24	0.9	Flex28	S	NH
SSD5	69	M	R	10	2	FlexSoft	S	Mild SNHL
SSD6	58	M	L	1	0.8	Flex28	S	NH
SSD7	41	F	R	12	1	Flex28	S	NH
SSD8	74	F	L	5	3	Flex28	S	NH
SSD9	65	M	L	7	3	Flex28	S	NH
SSD10	47	F	L	2	2	Flex28	S	NH
SSD11	64	M	R	1	4	Flex28	S	NH
SSD12	57	M	R	<1	0.8	Flex28	S	Moderate SNHL
SSD13	65	M	R	>10	0.6	Flex28	S	Mild SNHL
SSD14	60	M	L	21	4	CI24RE	P	NH
SSD15	46	M	L	<1	2	CI422	S	NH
SSD16	47	M	L	14	3	CI24RE	P	NH
SSD17	46	M	L	20	0.7	CI512	P	NH
SSD18	56	M	R	<1	3	CI512	P	NH
SSD19	68	M	L	<1	2	CI512	P	Moderate SNHL
SSD20	56	F	R	1.5	0.5	CI522	S	NH
SSD21	48	M	R	3	0.7	CI532	P	Mild SNHL
SSD22	60	M	L	6	1	CI532	P	Mild SNHL
SSD23	35	F	R	<1	0.6	CI622	S	NH

NH, Normal hearing; SNHL, sensorineural hearing loss; P, precurved; S, straight.

aid in everyday listening situations but did not use the hearing aid in the experiments described here. Testing was performed at the University of Maryland, College Park and Walter Reed National Military Medical Center in a quiet sound booth. The institutional review boards at each institution approved this research protocol. Informed consent was obtained from subjects before testing. Neither deception nor coercion was used in the study. Subjects were paid for their participation.

Interaural-time-difference discrimination
An ITD-sensitivity tuning curve was measured using electric pulse trains delivered to a single CI electrode or band-limited acoustic pulse trains delivered to an acoustic-hearing ear. The general methodology was to present a pulse train to one fixed electrode in the reference ear and to measure ITD sensitivity as a function of electrode number (BI-CI subjects) or acoustic carrier frequency (SSD-CI subjects) in the other comparison ear to identify the case that yielded the best ITD sensitivity. The reference ear was the functionally poorer ear as measured by sentence-perception scores in quiet (Goupell et al., 2018), and this ear was held fixed for each subject throughout all experiments. This was done with the idea that the data might ultimately be used to modify the frequency-to-electrode allocation to reduce interaural-place mismatch, and modifying the poorer (reference) ear would avoid disrupting speech cues in the ear that a subject generally relies on more heavily. The reference ear was always the CI ear for SSD-CI subjects. Within this general framework, it
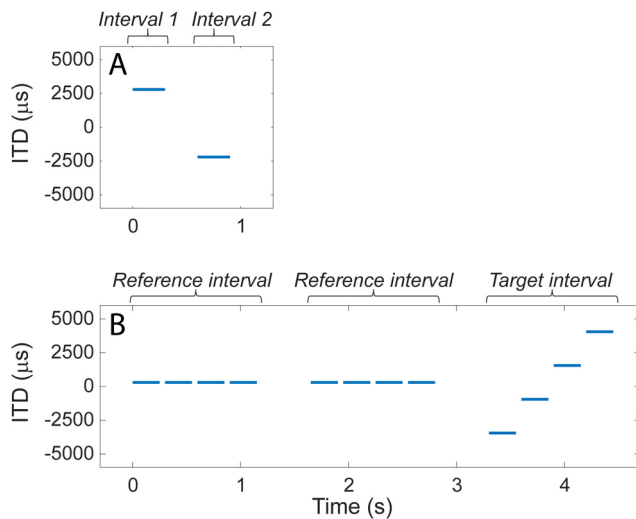
Figure 1. Examples of an ITD-discrimination trial. ***A***, For BI-CI subjects, a two-interval, two-alternative forced-choice left/right discrimination task required the subject to determine whether the two stimuli were played left then right or right then left. ***B***, For SSD-CI subjects, the left/right discrimination task proved too difficult given the inherent time delay between the ears. Therefore, a three-interval, two-alternative forced-choice task was used, which required the subject to determine whether the second or third interval contained a moving set of stimuli.

was necessary to use different methodologies for the ITD sensitivity task across the two subject groups (Fig. 1).

BI-CI subjects. The BI-CI subjects performed a two-interval, two-alternative forced-choice task that generally followed Kan et al. (2015). Two binaural 300-ms equal-amplitude pulse-train stimuli were presented sequentially, separated by an interstimulus interval of 300 ms (Fig. 1A). The two binaural stimuli had the same ITD magnitude, but the ITD was applied in opposite directions (e.g., one stimulus was right-leading, the other left-leading). Subjects were asked to determine whether the stimulus was perceived as moving from left to right or from right to left.

For most subjects and reference electrodes, an adaptive procedure was used to estimate the minimum ITD for which left/right discrimination was possible (i.e., the discrimination threshold). Discrimination thresholds were defined based on the relative ITD between the two intervals in the task (i.e., a 5000-µs ITD represents a condition where the ITD was +2500 µs in one interval and −2500 µs in the other, as shown in the example in Fig. 1A). For a given reference/comparison electrode pair, the starting ITD was usually 5000 µs but in a few cases was 2500 µs. The ITD magnitude then changed from trial to trial, following a three-down, one-up tracking rule (Zwislocki and Relkin, 2001) to estimate the 75% correct point on the psychometric function. The ITD changed by a factor of 2 until the second reversal, a factor of 1.414 until the fourth reversal, and a factor of 1.2 thereafter, with the ITD values rounded to the nearest 20 µs. For ITDs below 200 µs, the adjustment step size was fixed at 20 µs. The track continued for a total of 10 reversals, and the discrimination threshold was estimated as the geometric mean of the ITD for the last 6 reversals. At least three adaptive tracks were completed for each combination of reference and comparison electrodes, except when time constraints allowed only one run (5% of electrodes tested) or two runs (5%). In conditions where the SD of the ITD-discrimination threshold was >25%, we added two additional tracks, time permitting. The final threshold was computed by taking the geometric average of all completed tracks.

For a small number of initial cases (three subjects and two reference electrodes each, constituting ~5% of the data collected), a method of constant stimuli was used to estimate ITD-discrimination thresholds, although we moved away from this approach because it was too time consuming. For these measurements, ideally 50 trials were presented for each of a range of ITDs that produced a well-defined psychometric function, typically four points covering the range from near-chance to near-

perfect performance. ITD values typically started as 200, 400, 800, 1600 µs, but were then adjusted between 20 and 4000 µs depending on the sensitivity of the subject. Fewer trials (but always at least 36 per condition) were sometimes necessary given time constraints. Psychometric functions were fit to the data describing the percentage correct as a function of ITD, and the discrimination threshold was estimated based on the 75% correct point on this function.

Each subject performed a series of ITD-discrimination estimates for up to five electrodes in the reference ear (time permitting). For most subjects, the five electrodes chosen (of the 22 electrodes in the array) were E4 (near the high-frequency basal end of the array), E8, E12, E16, and E20 (near the low-frequency apical end of the array). In some cases where a subject had one of these electrodes deactivated (e.g., it was extra cochlear, it caused facial-nerve stimulation, or it produced an unpleasant auditory sensation), a different nearby reference electrode was selected. For a given reference electrode, the range of comparison electrodes was initially selected to include every even-numbered electrode within ±8 electrodes of the number-matched equivalent (e.g., for reference electrode E10, the range of comparison electrodes was E2–E18; for E4, the range was E2–E12). Additional even-numbered comparison electrodes and measurements were added until the subject could not reliably perform the task (>4 incorrect responses in a single block for an ITD of 5000 µs).

Electrical stimulation was presented using direct-stimulation research equipment and software, consisting of a pair of Nucleus Freedom Programming Pods, L34 sound processors, and Nucleus Implant Communicator (NIC2) software (Cochlear Ltd.) controlled by custom MATLAB scripts (MathWorks). Most subjects were presented with constant amplitude, 100 pulses-per-second (pps) monopolar pulse trains to one electrode in each ear, using biphasic pulses that were 58 µs in duration (25-µs anodic and cathodic phases separated by an 8-µs interphase gap). In some cases, pulse duration (30–50 µs) or stimulus rate was increased (200 pps) when the researcher had difficulty achieving comfortably loud stimulation levels. Synchronization was achieved via a trigger signal delivered from one pod to the other.

Before the experiment, loudness balancing was conducted to ensure that stimulation was presented at a comparable loudness level for each electrode. The loudness-balancing procedure was conducted in three steps. In the first step, the electrodes were monaurally loudness balanced within each ear. Subjects were asked to identify a comfortable loudness level for each individual electrode stimulated in isolation while ignoring the pitch of the stimulation. Then, subjects were presented with stimulation on five sequential electrodes and asked to judge whether there were any notable loudness differences among the five stimuli. Adjustments were made to the levels of the individual electrodes, and the five-electrode sweep was repeated until the subject reported that the five electrodes were comparable in loudness. This process was repeated with different selections of five electrodes until all available electrodes were loudness balanced. In the second step, electrodes were interaurally balanced across ears by using bilaterally sequential simulation for number-matched pairs of electrodes. In the third step, sound images for bilaterally simultaneous stimulation were centered for number-matched pairs of electrodes. Adjustments were made to the levels of the reference electrodes to intracranially center the sound image for each number-matched pair while keeping the nonreference ear electrodes loudness balanced within that ear. The three-step procedure was necessary because loudness-balanced stimuli do not necessarily produce a centered auditory image for stimulation presented simultaneously to both ears (Fitzgerald et al., 2015).

SSD-CI subjects. For the SSD-CI subjects, the procedure was as described by Bernstein et al. (2018) and some of the ITD-discrimination data reported here were previously reported in that study. The fact that one ear was electrically stimulated while the other was acoustically stimulated meant that there was an unknown relative delay in the time between stimulus presentation and auditory nerve response in each ear (Zirn et al., 2015). This made it difficult to create stimuli with equal but opposite effective ITDs as was done for the BI-CI subjects, thus complicating this approach. Although procedures have been developed using

auditory brainstem responses (Zirn et al., 2015) or psychophysical image centering (Francart et al., 2018) to determine this relative delay, the amount of time needed for these procedures was not feasible for the purposes of the current study because of the need to find this point for numerous reference comparison locations (Bernstein et al., 2018). Thus, instead of requiring SSD-CI subjects to discriminate the perceived direction of an interaurally delayed stimulus, the current study asked them to detect a change in ITD in a three-interval, two-alternative forced-choice task. The same procedure was not applied to the BI-CI subjects because the two-interval left/right discrimination task was feasible for those subjects and is much more efficient.

On each trial (Fig. 1B), SSD-CI subjects were presented three intervals separated by 500 ms, with each interval containing four binaurally presented 250- or 300-ms pulse-train bursts (duration held constant for each subject), each separated by 50 ms. In each of the two reference intervals, the four bursts all had the same ITD. In the target interval, the ITD varied among the four bursts. Subjects were instructed to identify which of the three intervals contained the stimulus that was moving or changing. The first interval was always the reference, and the subject was required to identify whether the target stimulus occurred in the second or third interval. The ITDs for the four bursts in the target interval were evenly spaced and symmetrically placed around the fixed ITD in the reference interval. For example, if the reference interval ITD was fixed at 500 μs for all four bursts, and the ITD spacing between bursts in the target interval was 2500 μs, then the four target-interval ITDs were -3250, -750, 1750, and 4250 μs (Fig. 1B). The pulse rate was in most cases 100 pps. For some reference electrodes for some subjects, the pulse rate was instead set to 50 pps, either because the subject was unable to detect ITD changes at 100 pps or because acoustic carrier frequencies below 1000 Hz were being tested (see below).

Electrical stimulation was delivered to the desired CI electrode using one of two methods depending on the CI manufacturer. For the SSD-CI subjects who used Cochlear-brand devices, the same direct-stimulation interface described above for the BI-CI subjects was used. The only difference was that synchronization of the electric and acoustic channels was achieved by initiating electrical stimulation via a trigger delivered from the second channel of a sound card (Hammerfall Multiface II, RME) that was used to generate the acoustic stimulus in the other ear. The trigger signal was amplified (HB7, Tucker-Davis Technologies) before being delivered to the programming pod. Interaural timing was calibrated by time-aligning the center of the acoustic pulse (at the headphone transducer) to the center of the electric pulse at the electrode, as measured using a Cochlear Freedom Implant Emulator containing a CI internal device and resistive load that approximated the impedance inside the human cochlea.

For the SSD-CI subjects who used MED-EL devices, electrical stimulation was delivered via auxiliary input to an Opus 2 processor that was programmed with up to four different single-channel maps. Each single-channel map was created by reducing the stimulation levels to zero for all channels except for the stimulated electrode, then setting the frequency cutoffs to the widest possible range allowed by the clinical software (5049–8010 Hz). The stimulation electrode was then selected by choosing the appropriate program using the remote control. An acoustic pulse train (see below) with a center frequency of 6529 Hz and a bandwidth equivalent to 1.5 mm on the Greenwood (1990) scale (1386 Hz), at the same pulse rate as the acoustic stimulus in the other ear, was then delivered to the auxiliary input of the processor.

Acoustic stimulation was delivered via circumaural headphones (HD 280 Pro, Sennheiser) to the desired cochlear place in the nonimplanted ear also as described by Bernstein et al. (2018). The acoustic stimuli consisted of trains of Gaussian-envelope pulses (Goupell et al., 2010, 2013), also known as Gabor (1947) pulses, constructed by modulating a sinusoidal carrier tone by a Gaussian-shaped envelope. The acoustic pulses were presented at the same rate as the electrical pulses in the other ear and had a -3-dB bandwidth equivalent to 1.5 mm on the Greenwood scale. The acoustic carriers were selected from a fixed set of frequencies, defined in 1.5-mm steps on the Greenwood scale (473, 616, 791, 1007, 1272, 1598, 2000, 2494, 3102, 3850, 4770, 5901, 7294, 9007, and 11,114 Hz).

The combination of pulse rates and carrier frequencies that could be reliably presented to subjects was limited by the physics of the stimulus generation and by the resolving capabilities of the cochlea. Because the bandwidth (in Hz) decreased with decreasing carrier frequency, this meant that the temporal width of the pulses (inversely proportional to the bandwidth) become larger with decreasing frequency. In most cases, subjects were presented with 100-pps pulse trains. However, at this rate, successive pulses would have overlapped by $>1\%$ in linear amplitude for carrier frequencies below 1140 Hz (Goupell et al., 2010). Furthermore, for low carrier frequencies, frequency components below about the 10th harmonic are resolved by the auditory system (Bernstein and Oxenham, 2003) and do not fall into the same auditory filter to generate an envelope at the desired pulse rate. This means that for a pulse rate of 100 pps, the intended pulse envelope would not be well represented for frequencies below $\sim$1000 Hz. Therefore, for relatively apical (i.e., low-frequency) reference electrodes where acoustic carrier frequencies $\leq$1000 Hz were included in the set of comparison stimuli, a lower pulse rate of 50 pps was used.

Subjects were generally tested on three different reference electrodes in the CI ear, although some subjects were tested on four or five electrodes when time permitted. For each reference electrode, ITD discrimination was measured for a range of at least 5, and in most cases 6–10, carrier frequencies for the acoustic pulse trains delivered to the other ear, with at least 30 trials per condition. For each electrode, several parameters of the electric and acoustic pulse trains and the range of acoustic carrier frequencies were adjusted in pilot tests. The goal was to identify a stimulus that would yield a maximum level of performance in the range of 80–90% correct, which would be high enough to estimate a tuning function while avoiding ceiling effects. The parameters that were adjusted included the following: the reference-interval ITD, the spacing between the ITDs in the target interval, the pulse rate, and the burst duration. Following Bernstein et al. (2018), the default values for these parameters depended on the CI manufacturer.

Before the experiment, sequential loudness balancing was conducted for each of the reference electrodes and acoustic carrier frequencies tested in the study. Perceptual centering for simultaneously presented bilateral stimuli was not conducted because this process was likely to be affected by both the relative interaural level and the time delay between the acoustic and electrical stimulation. Electric and acoustic stimuli were presented sequentially and the subject was asked to indicate which stimulus was perceived as louder. The experimenter then adjusted the level of the stimulus presented to one ear in steps of 1–3 dB (or in steps of 1–5 clinical current units for direct electrical stimulation) until the subject reported that the two stimuli were at equal loudness. For a given reference electrode, subjects were first presented with an acoustic pulse train with a carrier frequency of 2000 Hz and a level of 50–60 dB SPL, and the level of the electrical stimulus was adjusted to create a loudness match. Then, the electrical stimulus was held fixed at that level, and the levels for each individual acoustic carrier frequency were adjusted to create a loudness match to the electrical stimulus. In cases where a loudness match could not be reached within the limits of the system, which sometimes occurred for the highest frequencies tested, the level of the electrical stimulus was reduced and the loudness-balancing procedure was repeated for that reference electrode.

Analysis. For both subject groups, the ITD tuning curves were fit with a skewed-Gaussian function with four free parameters describing (1) the peak performance (best discrimination threshold or percentage correct), (2) the width, (3) the skewness of the function, and (4) the comparison electrode or frequency where this peak occurred (Bernstein et al. 2018). This fourth quantity served as the estimate of the interaural match (i.e., the comparison-ear electrode or acoustic frequency that yielded maximum performance). For the BI-CI subjects, chance performance for the purposes of curve fitting was taken to be the maximum allowed ITD in the adaptive track, which was either 2500 or 5000 μs. For the SSD-CI subjects, chance performance for the purposes of curve fitting was taken to be 50%.

Pitch ranking

To estimate the perceived relative place pitch between the two ears, this experiment used the midpoint comparison pitch-ranking methodology (Long et al., 2005; Cosentino et al., 2016), which involves a series of pitch

comparisons between two sequential sounds presented to different cochlear places. Sometimes the two sounds were presented to opposite ears (one ear and then the other), and sometimes to two cochlear locations in the same ear (one electrode and then the other). This technique was developed as a fast way to pitch rank a set of electrodes in the two ears and was found by Jensen et al. (2021) to yield a set of place-pitch estimates for BI-CI subjects that are relatively immune to procedural bias effects—including the influence of comparison-electrode test range and the starting point of an adaptive track—on the pitch-match estimate (Carlyon et al., 2010; Goupell et al., 2019). Although there were some differences in how this methodology was conducted for the BI-CI versus SSD-CI subjects (see below), the algorithm was generally similar for the two groups. Subjects were asked to pitch rank a set of stimuli consisting of a subset of electrodes or acoustic pure tones from each ear. This was accomplished through a series of pairwise comparisons, where each new electrode or pure tone (the new stimulus) added to the ranking was compared with the existing ranking in an adaptive manner. First, the new stimulus was compared in pitch (higher/lower) to one of the already-ranked electrodes or pure tones. Based on the subject's response, the possible choices for ranking position of the new stimulus were reduced to only those electrodes/tones that were either higher or lower in pitch rank than this particular already-ranked stimulus. The next already-ranked stimulus to be compared with the new stimulus was then chosen to be the midpoint of this new reduced range. This process was repeated iteratively until the stimulus choices were exhausted, and the new stimulus was assigned to a position in the ranking. Then the process was repeated with each new stimulus until the full set of stimuli was ranked. The ranking process was repeated 10 times for each subject.

BI-CI subjects. The BI-CI subjects pitch ranked all even-numbered electrodes from the two ears (up to a total of 22 electrodes, 11 for each ear). Single 300-ms bursts of a 1000-pps pulse train were presented sequentially to two successive electrodes with an interstimulus interval of 300 ms. In each block, the subjects were initially presented with two sequential bursts on two different electrodes chosen at random, and their response regarding which electrode was higher established the rank order for these two electrodes. Then, a third electrode was compared with one of the two electrodes in the existing ranking, chosen at random. Depending on the response, it might then have been compared with the other electrode in the existing ranking to establish a ranking of the three electrodes. Subsequent electrodes were added into the ranking one at a time, as described above, until all 22 electrodes were pitch rank ordered. Note that because this algorithm rank ordered the electrodes from both ears, some trials involved across-ear sequential comparisons (one stimulus in each ear), and some trials involved within-ear sequential comparisons (both stimuli in one ear).

SSD-CI subjects. Sequentially presented single 300-ms bursts of sounds (now pulse trains and pure-tone bursts) were presented with an interstimulus interval of 300 ms. There were two considerations that required changes to the pitch-ranking protocol relative to the BI-CI subjects. The first consideration was that for the acoustic ear, the step sizes (1.5-mm spacing between adjacent stimulus frequencies) were so large relative to frequency-discrimination thresholds that subjects could rank order these pure tones with nearly perfect accuracy. Therefore, the acoustic tone frequencies were assumed to be perfectly rank ordered without testing, and individual CI electrodes were added into this rank ordering. The second consideration was that for the MED-EL subjects, the electrical stimulation on a given electrode was generated by presenting a pure-tone stimulus to the auxiliary input of the sound processor loaded with single-channel maps. Because the intended electrode was selected manually by changing the program with the remote control, and only four single-channel maps could be stored in a given processor, it was not possible to complete a full ranking of the electrodes and acoustic frequencies.

Therefore, to keep the procedure as similar as possible between the Cochlear-brand and MED-EL users, all the SSD-CI subjects were tested in a modified pitch-ranking methodology where only one electrode at a time was ranked relative to the fixed set of acoustic frequencies. For the Cochlear-brand subjects, up to 11 different electrodes were tested using direct stimulation. For the MED-EL subjects, up to seven different electrodes were tested using this methodology by loading four single-

electrode maps to one sound processor and another set of three single-electrode maps to a second sound processor. Five pitch-ranking blocks were completed for each single electrode before changing the map to test a different electrode. This process was completed twice for a total of 10 pitch-ranking blocks per electrode.

Analysis. To quantify the interaural pitch match, the goal of the analysis was to identify the comparison-ear electrode number or acoustic frequency that was best pitch matched to a given reference-ear electrode. For the BI-CI subjects, the data were analyzed by plotting the average rank (among the 22 electrodes tested) for each of the 11 electrodes tested in each ear, then fitting the data for each ear with a sigmoidal function. For a given reference-ear electrode, the matching comparison-ear electrode was identified by choosing the comparison-ear electrode that yielded the same average rank as determined by the functional fits.

For the SSD-CI subjects, the pitch-ranking data were analyzed to determine which pure-tone frequency was most closely matched to a given CI electrode. Because the acoustic pure tones were assumed to be correctly rank ordered, fitting was not required to extract this information from the ranking data. For each pitch-ranking block, the best-matching frequency was defined to be the midpoint (on the Greenwood scale) between the two frequencies above and below the CI electrode in the ranking. The matched frequency was then determined by averaging (on the Greenwood scale) the 10 blocks for each electrode.

Bias checks. Carlyon et al. (2010) argued that interaural pitch-match estimates can be influenced by the parameters of the available comparison-ear stimuli rather than the perceived pitch of the electrode of interest in the reference ear. They proposed checks that could be conducted to verify a minimal effect of such influences. For an adaptive pitch-matching procedure, they proposed that a pitch match can be considered valid if it is relatively immune to changes in the starting point of the adaptive track. They proposed a criterion ratio of 0.5; in other words, for a given change in the starting point of the adaptive track, a pitch match is considered valid if it changes by less than half that amount. For each electrode tested, the slope of the relationship between the pitch rank and the adaptive track starting point was calculated. For the BI-CI subjects, the mean slope was −0.03 (±0.33 SD) and 4.7% of electrodes tested had slope >0.5. For the SSD-CI subjects, the mean slope was 0.05 (±0.17 SD), and 1.7% of electrodes tested had slope >0.5. Thus, nearly all the pitch matches passed the starting-point bias check.

Computed-tomography scans

CT scans can provide precise physical electrode-location information in terms of insertion depth, modiolar distance, and scalar location, and thus provide precise interaural-matching information. CT-based location estimates are more precise than perceptual or electrophysiological interaural-matching methods, which often show broad tuning, particularly for binaural sensitivity. They are also relatively quick to obtain and analyze compared with perceptual methods. Despite these advantages of CT scans, there are some disadvantages. First, subjects are exposed to additional and voluntary radiation. Our procedure exposes a CI user to an effective dose of 1.7 millisievert (mSv), which is within the typical range for a diagnostic CT scan (Mettler et al., 2020) and equivalent to ~7 months of exposure to natural background radiation such as terrestrial radon and cosmic rays (3.1 mSv/year; Wall, 2009). Although this exposure is relatively low for an adult, best medical practices recommend against elective use in a child where radiation exposure presents a higher risk (Goodman et al., 2019). Second, CT scans do not provide an assessment of functional performance, meaning that the individualized electrode-to-neural interface (Long et al., 2014), including the survival of the spiral ganglia, is not considered in the measurements.

CT scans of CI electrode locations were acquired on a multidetector row CT scanner with a special temporal-bone protocol that included extended Hounsfield unit scale implementation. Other scan parameters were 0.6-mm collimation, 140-kVp tube voltage, 300-mAs tube current (without modulation), 0.3-mm spacing between slices, and bone kernel for image reconstruction. In addition to standard temporal-bone images in the axial and coronal planes, a 10-cm field-of-view oblique Stenver reformat parallel to the basal turn of the cochlea was created for better

depiction of the electrode array position with ultra-high in-plane resolution of 0.2 × 0.2 mm.

Analysis. An automated image analysis sequence was used to determine the intracochlear location of the electrodes. A so-called statistical shape model (Cootes et al., 1995) of intracochlear anatomy based on the manual delineation of structures in micro CT scans from 16 cadaveric specimens (an increase from the 6 specimens reported in Noble et al., 2011) was used to determine patient-specific cochlea shape from CT scans. The model encodes typical nonrigid variations in cochlear anatomy. Once it is nonrigidly fitted to the cochlea shape in a new patient's CT, it allows an accurate estimate of the position of fine-scale internal cochlear structures that are not directly visible in the patient's CT. The model fitting of the cochlear structures was based on preimplantation images when available. When no preimplantation CT was available, either the mirror image of the opposite unimplanted cochlea (for SSD-CI subjects; Reda et al., 2014) or a machine-learning-based approach using the postimplantation CT alone (for BI-CI subjects; Wang et al., 2019) was used. The electrode array was localized in a postimplantation CT using automated algorithms (Zhao et al., 2019). The two results were then merged using well-known rigid image registration techniques (Maes et al., 1997) as has been validated in histologic studies (Schuman et al., 2010).

The modeling analysis quantified the estimated electrode position in the following dimensions (Verbist et al., 2010): (1) the insertion angle, which reflects the tonotopic location along the cochlear spiral, based on a coordinate system defined by a line drawn between the round window (0°) and the modiolus; (2) the distance between the electrode and the modiolus that contains the spiral ganglia (i.e., the modiolar distance); and (3) the scalar location of the electrode (i.e., whether it is located within scala tympani, within scala vestibuli, or in the in-between region designated as scala media or basilar membrane). In this study, the insertion angle was the main outcome measure of interest for the purposes of comparing estimates of interaural place mismatch. The insertion angle (in degrees), rather than the insertion depth (in millimeters), was used to define the tonotopic location of stimulation. This is because the relationship between the insertion angle and tonotopic frequency is thought to be relatively independent of the individual size of the cochlear duct and is also independent of the radial distance of the electrode from the modiolus (Stakhovskaya et al., 2007). For the BI-CI subjects, the matching comparison electrode for a given reference electrode was extracted by linearly interpolating the insertion-angle data, then finding the comparison electrode at the same insertion-angle as the reference electrode. For the SSD-CI subjects, the matching acoustic frequency for a given reference electrode was derived using the Stakhovskaya et al. (2007) spiral-ganglion correction to the Greenwood map.

Experimental design and statistical analysis
For each reference electrode, an estimate of the matched comparison electrode or comparison acoustic frequency was extracted for each of the three methods (ITD, CT, and pitch) as described above. Only those electrodes for which matching estimates were available for all three methods were included in further data analysis (because of its time-consuming nature, fewer electrodes were tested in the ITD experiment). For each method, the match in the comparison ear was converted into an equivalent insertion angle (see Results, Relationship among the three methods). Broadly speaking, mismatch was calculated in terms of the angular difference in the estimated places of stimulation in the two ears for a given acoustic frequency. For the BI-CI subjects, this estimate reflected the difference in relative locations for two electrodes tuned to the same frequency in the two ears. For the SSD-CI subjects, this estimate reflected the difference between the insertion angle of a given electrode and spiral ganglia tuned to the same frequency as that electrode.

All mismatch estimates were based on the frequency allocation in each subject's everyday sound processor(s). These allocations sometimes differed from the default recommendations of the manufacturer because of the presence of deactivated electrodes or a clinician's initiative. Analysis of the actual subjects' frequency allocations was important because the main research question was whether the perceptual estimates of interaural place stimulation would align more closely with the everyday frequency allocation (i.e., evidence that plasticity overcomes mismatch) or with the CT-estimated place of stimulation (i.e., no evidence of plasticity).

Three sets of analyses of interaural place mismatch were conducted using linear mixed-model regression (lmer function in Rstudio, version 1.2.5001). Main effects and interactions are reported in terms of χ^2 values describing the effect of removing the term of interest from each model. The first set of analyses compared CT estimates of electrode insertion angles and interaural place mismatch for the two groups. Because this initial analysis found that mismatch was rarely observed for the BI-CI subjects, but frequently observed for SSD-CI subjects, the remaining analyses considered the two groups separately. All individual subjects were included in the analyses as a random effect. Although there was variability in the brand, model, and type of electrode array across subjects and sometimes across ears (Tables 1, 2), there were insufficient counts for each possible combination to allow for a statistical evaluation of the effects. Therefore, no array variables were included as a factor in the analysis.

Between-group comparison of mismatch. The purpose of this set of analyses was to evaluate the differences in electrode location and interaural place mismatch between the two groups, as estimated using CT scans. These analyses included the absolute electrode insertion-angle or interaural-place mismatch (in degrees) as the outcome variable, tonotopic location (defined by the frequency allocation for a given reference electrode in the CI sound processor) as a fixed effect, and subject as a random effect.

Across-subject relationship among methods. The purpose of this set of analyses was to determine the extent to which each method yielded a similar estimate of mismatch. The magnitudes of the interaural place-mismatch estimates were compared in six mixed-model analyses, each making pairwise comparisons between two of the mismatch methods across the electrodes tested for a given subject group. Each model treated one mismatch estimate as the outcome variable, the other as a fixed effect, and subject as a random effect. Bonferroni corrections were applied for six comparisons (criterion, $p < 0.05/6 = 0.0083$).

Tonotopic dependence. The purpose of this set of analyses was to determine how the three estimates of mismatch varied as a function of tonotopic location along the electrode array. Linear mixed-model regression analyses examined the dependence of mismatch on the interaural matching method (ITD, pitch, or CT) for each subject group, with tonotopic location (defined by the frequency allocation for a given reference electrode in the CI sound processor) as a fixed effect, and subject included as a random effect, with Bonferroni corrections applied for two analyses (criterion, $p < 0.05/2 = 0.025$).

Results
Example individual results
Before presenting the group data, the raw data that formed the basis of the interaural place mismatch estimates are illustrated for three example BI-CI and three example SSD-CI subjects (Fig. 2). Each column in Figure 2 shows the data for one subject. These six individuals were chosen to highlight the range of outcomes revealed by the three methods. Figure 2, *A* and *B*, shows example results for ITD discrimination; Figure 2, *C* and *D*, shows example results for pitch ranking; Figure 2, *E* and *F*, shows example results for the CT scans. The bottom row (Fig. 2*G,H*) plots the estimates of the relative place of electrical stimulation for all three methods. The horizontal axes in Figure 2, *A*, *C*, and *D*, are arranged so that the lowest-frequency electrode toward the apex of the cochlea is on the left. For Cochlear-brand devices, the electrodes are numbered in descending order from 22 (low) to 1 (high frequency), whereas for the MED-EL device (SSD2), the electrodes are numbered in ascending order from 1 (low) to 12 (high frequency).

Interaural-time-difference discrimination
Figure 2, *A* and *B*, shows example ITD-discrimination tuning curves, with each diagram representing a different reference
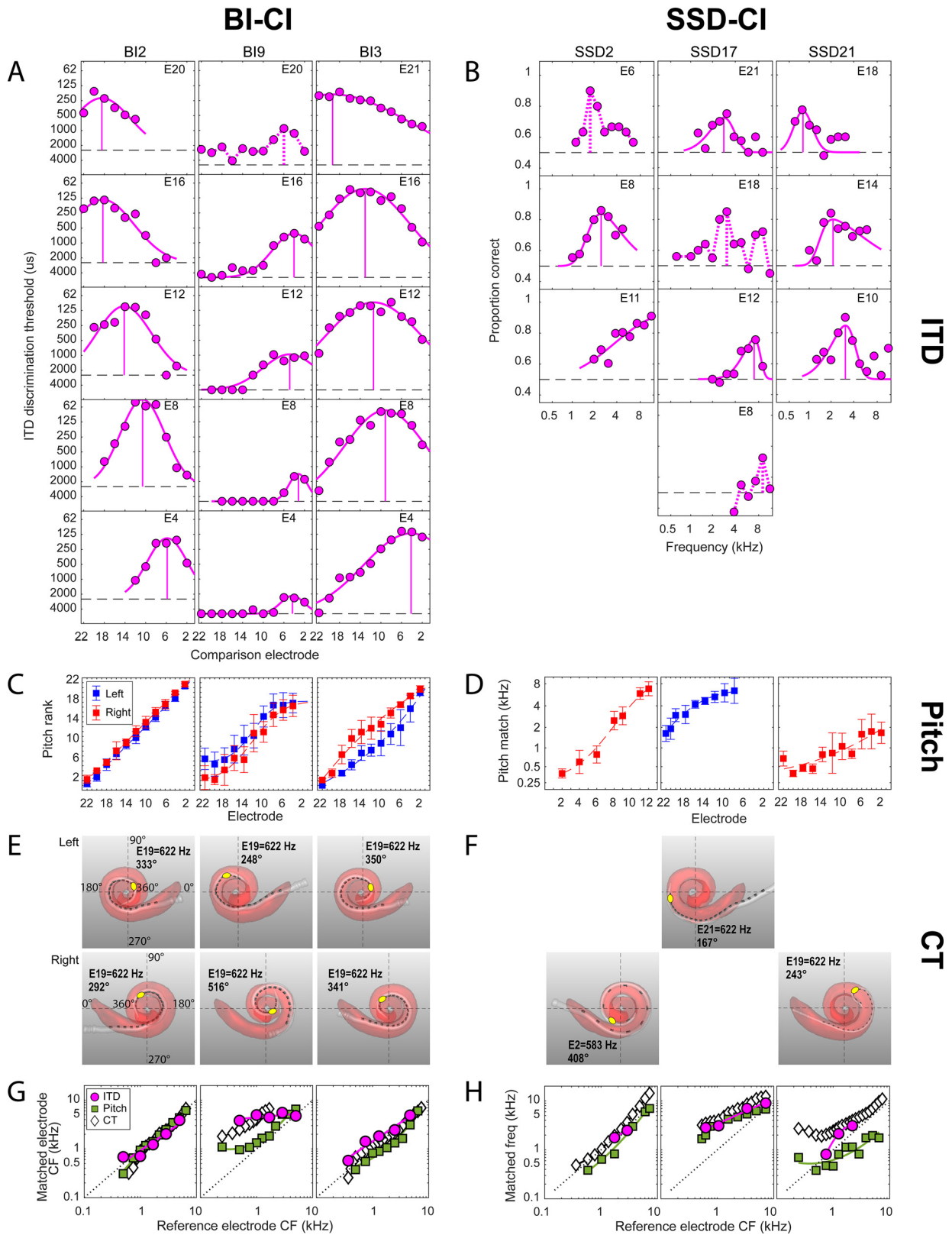
Figure 2. Examples of the perceptual and objective data collected for the three interaural place-mismatch estimation methods for six example subjects (3 BI-CI and 3 SSD-CI). For each subject, the reference ear is defined as the functionally poorer ear as determined by speech understanding scores. *A*, *B*, ITD discrimination data. Discrimination threshold (BI-CI subjects) or proportion correct (SSD-CI subjects) as a function of the comparison electrode or frequency for a given reference electrode. The dashed horizontal line shows where threshold could not be measured (*A*) or chance performance (*B*). The vertical line shows the estimated interaural place match. *C*, *D*, Pitch ranking data; rank (BI-CI subjects) or pitch match (SSD-CI subjects) as a function of electrode number. Error bars indicate the standard deviation of the rank or match. *E*, *F*, Computational model output of the CT scan analysis, showing the estimated cochlear morphology (red), the position of the electrode array (white), and the individual electrode contacts (dark gray). *G*, *H*, Summary of the three estimates of interaural place match as a function of reference electrode number (BI-CI subjects) or reference electrode CF (SSD-CI subjects) derived from the measurements in *A*–*F*. The diagonal dotted lines in *G* and *H* represent perfect interaural alignment; vertical displacement from this line represents mismatch.

electrode, arranged from top to bottom from apex (low-frequency electrode) to base (high-frequency electrode). For the BI-CI subjects, the individual graphs in Figure 2A indicate the ITD left/right discrimination threshold as a function of the comparison electrode number. For the BI-CI subjects, the group logarithmic mean best threshold (i.e., at the tip of the tuning curve) across the reference electrodes tested was 442 μs. For the SSD-CI subjects, the individual graphs in Figure 2B indicate the proportion-correct performance (in identifying the interval that contained an ITD that changed across the four bursts) as a function of the center frequency (CF) of the acoustic click train presented to the unimplanted ear. The ITD-discrimination threshold could not be ascertained for the SSD subjects because a fixed-ITD methodology was used to overcome the complications stemming from the interaural delay between the acoustic and CI ears (Bernstein et al., 2018).

The key parameter that was extracted from the fitted functions for further analysis was the comparison electrode or acoustic frequency that yielded peak performance, which is identified by solid vertical lines Figure 2, A and B. In some cases (6% of electrodes tested), there was a prominent peak in the performance function, but a skewed Gaussian curve could not be fit to the function. In these cases, the acoustic comparison frequency yielding a peak in the performance function was taken as the frequency-match estimate. These cases are identified by dashed vertical lines. There were also several cases (13% of electrodes tested) where no frequency-match estimate was made (Bernstein et al., 2018), either because the performance function showed no prominent peak, showed two or more peaks of similar amplitude, or suggested a peak outside the comparison range (for example, SSD2, E11 in Fig. 2B). These cases were discarded from further analysis.

Pitch ranking
Figure 2, C and D, shows example results for the pitch-ranking experiment. The BI-CI subjects jointly ranked all even electrodes in both ears. Therefore, there are two curves indicating the average rank for the electrodes in each ear in Figure 2C. For the BI-CI subjects, the pitch match for each electrode in the reference ear was derived by fitting sigmoidal curves to the data for each ear and then extracting from these fitted functions the comparison electrode that yielded the same average pitch rank as the reference electrode in question. Figure 2C shows a variety of outcomes for the pitch-matching task, from a case with very little mismatch (BI2, left column) to cases with substantial mismatch that either varied (BI3, right column) or was reasonably constant (BI9, middle column) across the array.

The SSD-CI subjects performed the pitch-ranking task for each reference electrode relative to a set of frequencies that was assumed to be correctly ordered in the acoustic ear. Therefore, there is only one pitch-ranking curve for each subject in Figure 2D. There was a wide variety of pitch-match estimates across these three example SSD-CI subjects. For subject SSD2 (left), the pitch matches across the array covered nearly the full range of comparison frequencies. For the other two subjects, the range of matches was limited to the upper (SSD17, middle) or lower (SSD21, right) portions of the comparison range.

Computed-tomography scans
A visual depiction of the CT-scan modeling analysis is shown for both ears for the three example BI-CI subjects (Fig. 2E) and for the implanted ear for the three example SSD-CI subjects (Fig. 2F). These images include the estimated cochlear morphology (pink shading) and the estimated locations of the array (white) and individual electrodes (dark gray) within the cochlea. These examples show a variety of insertion depths and mismatch. In each image, the insertion angle associated with an electrode programmed to a logarithmic center CF near 600 Hz is indicated by a yellow point to provide a visual reference. In most cases this was E19 (standard Cochlear Ltd. frequency allocation, 622 Hz) but differed for two subjects with nonstandard allocations (E21 = 622 Hz for Cochlear Ltd. subject SSD17; E2 = 583 Hz for MED-EL subject SSD2).

For the BI-CI subjects (Fig. 2E), these examples show variation in both the absolute insertion depth and the degree of mismatch in insertion depth between the two ears (i.e., interaural place mismatch). The left (BI2) and right (BI3) columns show an insertion of approximately one full turn that was similar between the two ears, yielding very little mismatch. The middle column (subject BI9) shows a deep insertion of more than a full turn in the right ear but a shallower insertion of about a full turn in the left ear. As a result, subject BI9 has 10–11 electrodes of interaural place mismatch (white diamonds in Fig. 2G), with E19 located at 248° in the reference (left) ear and 516° in the comparison (right) ear.

For the SSD-CI subjects, Figure 2F shows a relatively deep insertion greater than one full turn (SSD2, left column), a relatively shallow insertion of only about half a turn (SSD17, middle column), and a case of limited insertion depth because of a tip foldover (SSD21, right column).

Estimates of interaural place mismatch
Figure 2, G and H, plots the relative places of electrical stimulation as estimated by the three different methods. For both groups, the horizontal axis represents the geometric center of the frequency range to which each electrode in the array is mapped in the subject's sound processor. This quantity, referred to as the "reference-electrode CF," is used throughout the figures and analyses to place each electrode on a common reference based on a subject's own map of frequency-to-electrode allocations. Used in place of an electrode number, this characterization allows for the normalization of any differences in this allocation because of device brand, the presence of deactivated electrodes, or a clinician's initiative.

The vertical axis represents the CF allocated to the matching comparison electrode in the other ear for BI-CI subjects (Fig. 2G) or the matching acoustic frequency for SSD-CI subjects (Fig. 2H). The diagonal dashed line represents the 1:1 line of equality; in other words, where the matched comparison-electrode CF or acoustic frequency was equal to the reference-electrode CF. Points falling above the diagonal line indicate cases, that for a given stimulus frequency, the stimulated cochlear place was more basal (i.e., a higher-frequency cochlear place) in the reference ear than in the comparison ear. For the SSD-CI subjects, mismatch is expected to be in this basal direction as the array is generally not inserted deeply enough to stimulate the apical portion of the cochlear (Landsberger et al., 2015). For the BI-CI subjects, a mismatch could go in either direction, depending on the relative insertions in the two ears.

For the example subjects depicted in the left columns for each subject group in Figure 2, G and H (BI2 and SSD2), all three estimates were relatively consistent with one another, and there was little interaural place mismatch. For the example subjects depicted in the center columns for each subject group (BI9 and SSD17), all three methods showed substantial interaural place mismatch. For BI9, the three methods were not closely aligned, although all three suggested a mismatch. For SSD17, the three
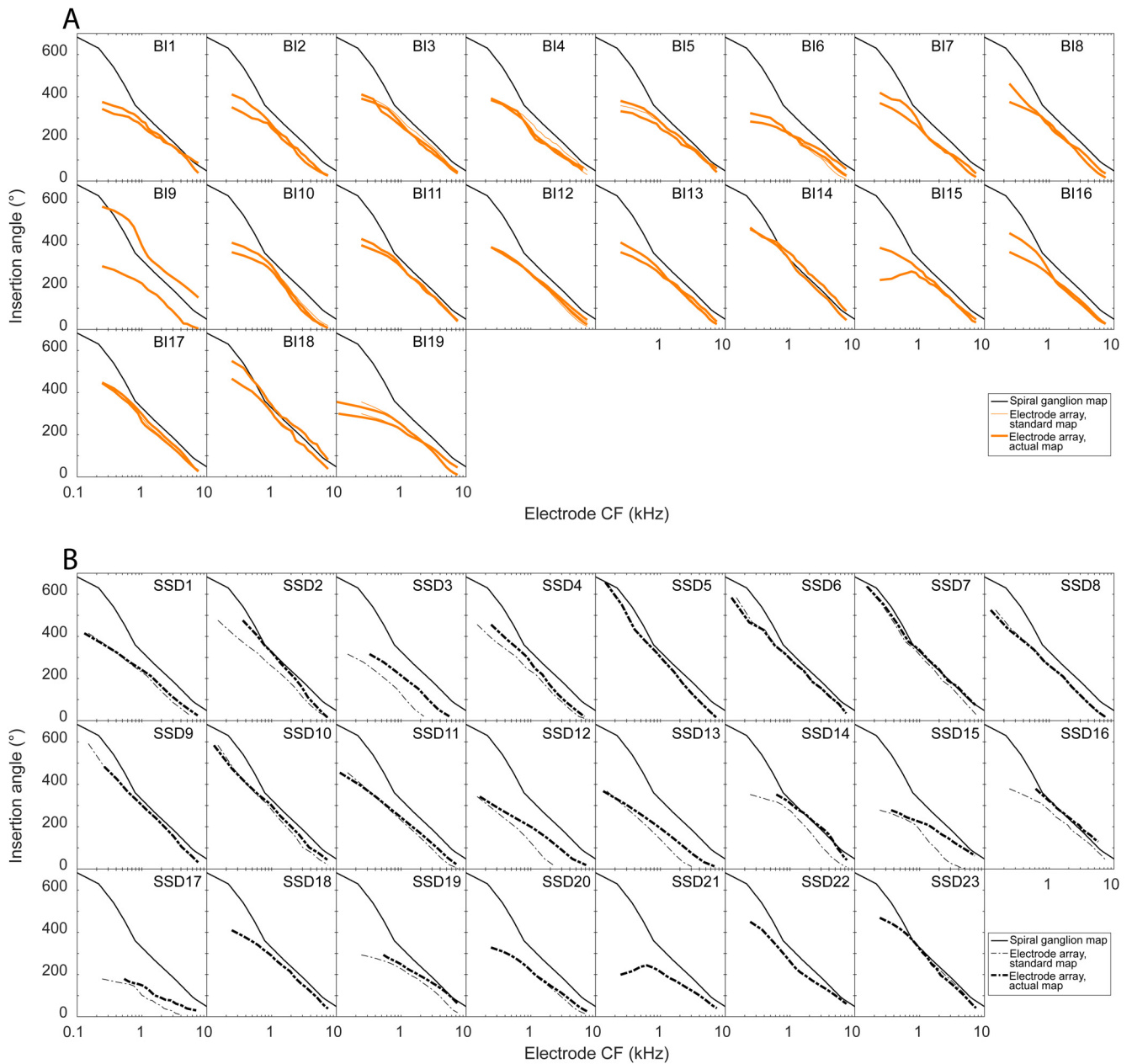
Figure 3. CT scan data for each individual subject in the study showing the absolute insertion angles of each electrode in the array for the BI-CI subjects (*A*) and the SSD-CI subjects (*B*). The thin lines plot the insertion depth as a function of the specific default frequency allocation for each electrode from the manufacturer. The thick lines plot the insertion angle as a function of the subject's actual frequency allocation, which differs in some cases from the default of the manufacturer. The solid black line is an absolute reference line depicting the relationship between the electrode insertion angle and the spiral ganglion characteristic frequency at that location (Stakhovskaya et al., 2007).

methods showed similar estimates of electrode position. For the example subjects depicted in the right columns for each subject group (BI3 and SSD21), the three methods suggested different mismatch results. For BI3, the ITD and pitch methods suggested some mismatch, but in opposite directions, whereas the CT scan suggested little or no mismatch. For SSD23, the CT scan suggested substantial mismatch, the pitch method suggested mismatch in the opposite direction, and the ITD method suggested a mismatch that was similar to the CT scan for two of the electrodes tested, but no mismatch for the third electrode.

Radiographic data

To examine the variability in electrode placement and to illustrate how this placement results in interaural place mismatch,

Figure 3 plots the absolute insertion angles from the CT scans as a function of the frequency at the geometric center of the frequency range to which each electrode in the array is mapped. The subject's actual frequency allocation that formed the basis of all mismatch analyses is represented by a thick line (Fig. 3*A*, solid orange for BI-CI subjects; Fig. 3*B*, dotted black for SSD-CI subjects). In cases where this differed from the standard allocation of the manufacturer, the standard allocation is represented by a thin (solid orange or dotted black) line to illustrate what the mismatch would have been without these changes. Also plotted in Figure 3 is the Stakhovskaya et al. (2007) map, which represents the characteristic frequency of spiral ganglia located at a given insertion angle (solid black line).
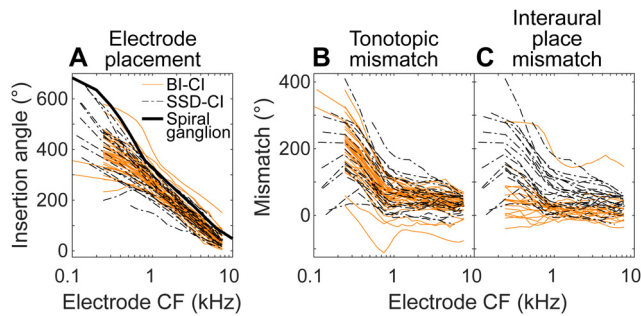
Figure 4. *A*, Comparison of the absolute electrode positions for the BI-CI (orange) and SSD-CI subjects (black) as a function of the actual frequency allocation of the electrode. *B*, The tonotopic mismatch between the insertion angle and the electrode frequency allocation was similar for the two groups. *C*, The interaural place mismatch, which reflects the relationship between the two electrode insertions for the BI-CI subjects but reflects the tonotopic place mismatch for the SSD-CI subjects, was smaller for the BI-CI subjects.

For the BI-CI subjects (Fig. 3*A*), interaural place mismatch is characterized by the vertical displacement between the two electrode arrays (thick solid orange lines). There tended to be little mismatch between the two arrays, except for some mismatch near the apex. In one case with large interaural place mismatch (BI9), Figure 3*A* suggests that this mismatch arose because of an abnormally deep insertion in one ear. In contrast, interaural place mismatch for the SSD-CI subjects (Fig. 3*B*), who have a CI in one ear and acoustic hearing in the other, is characterized by the vertical displacement between the electrode array (thick dashed black lines) and the spiral ganglion map (solid black lines). Because the apical end of the electrode array does not reach the apex of the cochlea, but the most apical electrode is typically programmed to deliver low-frequency information (~100–200 Hz), this leads to interaural place mismatch in most cases.

Figure 3 shows that in most cases for both groups, the arrays were mismatched from the spiral ganglion map. Figure 4*A* plots the insertion angles for all 38 BI-CI ears (solid orange lines) and 23 SSD-CI ears (dashed black lines) relative to the allocated frequency of each electrode. A repeated-measures mixed-model regression analysis was conducted on the insertion-angle data, with two fixed-effect variables (group and electrode log-CF) and subject as a random variable. There was a significant main effect of log-CF [χ^2 (1) = 723, $p < 0.0001$], as expected (because lower-frequency electrodes are located more apically on the array), but there was no significant effect of group [χ^2 (1) = 0.33, $p = 0.56$] or group × log-CF interaction [χ^2 (1) = 0.89, $p = 0.34$]. This means that there was no difference between the groups in terms of the mismatch between the electrode location and cochlear tonotopy (tonotopic mismatch; Fig. 4*B*).

Despite the similar tonotopic mismatch observed for the two groups, interaural place mismatch was different for the two groups because of a key anatomic difference. For the BI-CI subjects, interaural place mismatch is determined by the relative locations of electrodes tuned to the same acoustic frequency in the two ears; tonotopic mismatch between electrode placement and the spiral-ganglion map is irrelevant. For the SSD-CI subjects with acoustic hearing in one ear, interaural place mismatch is directly determined by the tonotopic mismatch.

Figure 4*C* plots the interaural place mismatch for both groups. (Note that this was equal to the tonotopic mismatch in Fig. 4*B* for the SSD-CI subjects, but not for the BI-CI subjects.) The sign convention was established to produce, on average, a positive mismatch for each subject. For each BI-CI subject, the

positive direction was defined based on the average mismatch across the array. For each SSD-CI subject, the positive direction was defined by the expected direction of the mismatch, based on the assumption that the cochlear place of electrical stimulation would generally be basal (i.e., higher frequency) to the CF-equivalent place (Landsberger et al., 2015). The larger interaural place mismatch observed for the SSD-CI subjects was confirmed by a mixed-model regression analysis conducted on the interaural mismatch estimates. There were significant main effects of group [χ^2 (1) = 11.9, $p = 0.0006$] and frequency allocation [χ^2 (1) = 286, $p < 0.0001$]. There was also a significant interaction between the two variables [χ^2 (1) = 139, $p < 0.0001$], reflecting the larger group differences for low-frequency electrodes where the SSD-CI subjects experienced the largest interaural place mismatch.

In summary, Figure 4 shows that there were no group differences in electrode placement. Instead, the larger interaural place mismatch for the SSD-CI subjects stems from a fundamental anatomic distinction; BI-CI mismatch reflects the relative placement of two arrays, whereas SSD-CI mismatch reflects the absolute placement of one array relative to the tonotopy of the cochlea.

Relationship among the three methods
Individual data
Figure 5 plots estimates of interaural place-of-stimulation mismatch for all three methods for each individual subject. These plots, shown here for all 19 BI-CI and 23 SSD-CI subjects, are similar to the summary plots for the example subjects in Figure 2, *G* and *H*, and follow the same plotting conventions.

Several trends are apparent in these individual data. For the BI-CI subjects, most of the place estimates fell close to the diagonal (except for subject BI9), consistent with the relative lack of mismatch observed in the CT results (Fig. 4*C*, solid orange lines). For the SSD-CI subjects, most of the estimates fell above the diagonal line, consistent with the mismatch observed in the CT results (Fig. 4*C*, dashed black lines). Second, the CT (white diamonds) and ITD (magenta circles) estimates were generally consistent with one another. For the BI-CI subjects, they both fell near the diagonal in most cases, indicating little interaural place mismatch, whereas for the SSD-CI subjects, these two estimates tended to have a similar slope and show a similar degree of excursion from the diagonal. There were, however, exceptions. For example, the CT scan suggested a large mismatch, but the ITD method did not for subject SSD11. Third, the pitch estimates (green squares) were much more variable than, and were often inconsistent with, the other two methods. For the BI-CI subjects, there were a number of cases where the CT and ITD methods suggested little or no mismatch, whereas the pitch method suggested substantial mismatch (e.g., subjects BI4 and BI11). For the SSD-CI subjects, the pitch estimates were in general lower than the other two estimates and with a more gradual slope, suggesting a positive mismatch for more apical electrodes and a negative mismatch for basal electrodes.

Group data
To compare the three methods, the ITD-based (dITD), pitch-based-based (dPitch), and CT-based (dCT) estimates of interaural place mismatch were defined for a given reference electrode as the distance between the cochlear locations associated with each estimate and the reference-electrode CF. All mismatch estimates are expressed in terms of insertion angle. For the BI-CI subjects, the comparison-ear CT scan formed the basis of the translation between the electrode number and insertion angle. Mismatch was calculated by comparing the insertion angle of the
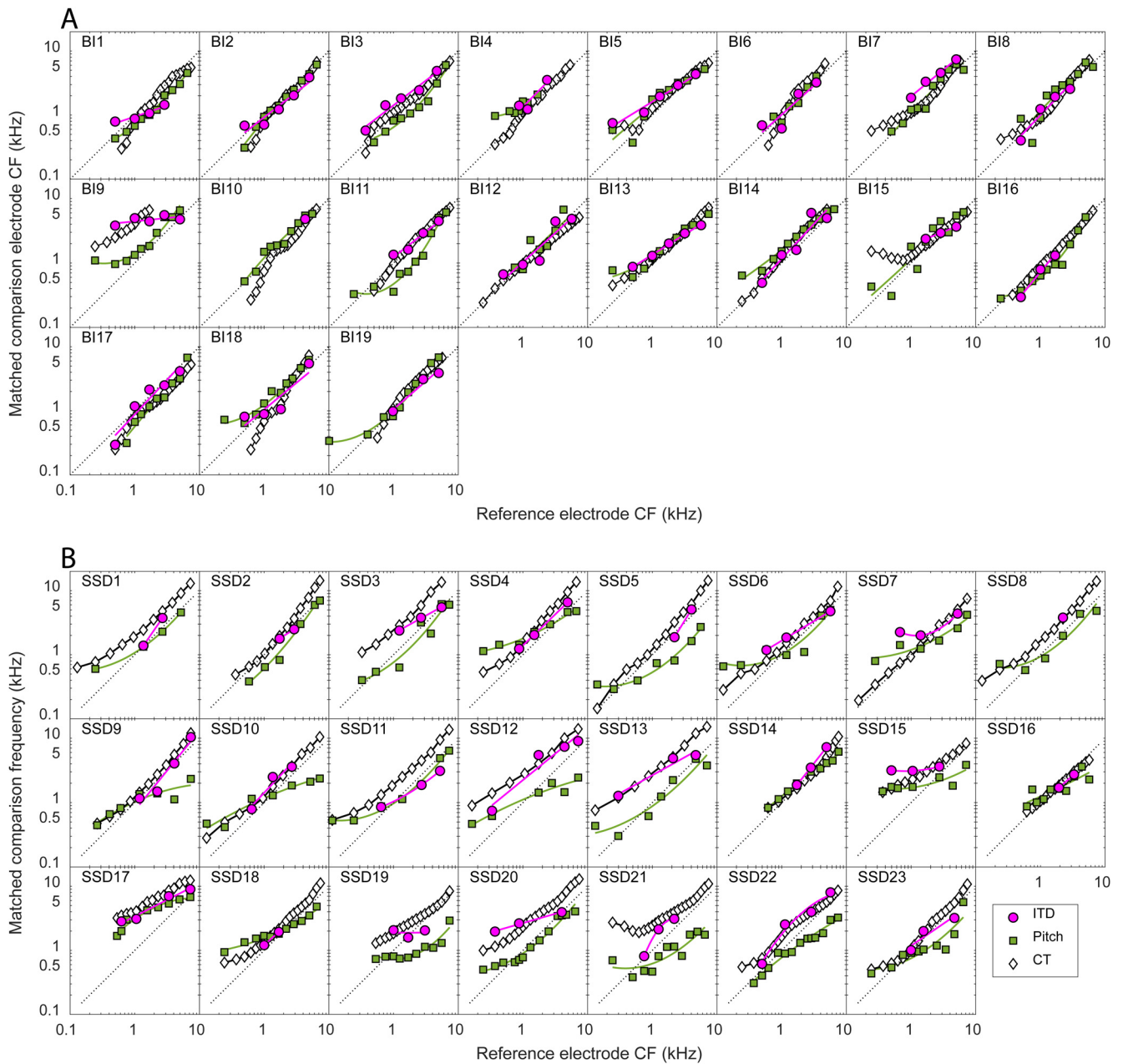
Figure 5. Summary of the three estimates of relative interaural place for each individual subject in the study. ***A***, For the BI-CI subjects, the matched electrode in the comparison ear is plotted as a function of the reference electrode. ***B***, For the SSD-CI subjects, the matched acoustic frequency in the comparison ear is plotted as a function of the reference electrode CF. The diagonal dotted lines represent perfect interaural alignment; vertical displacement from this line represents mismatch.

matched comparison electrode to the insertion angle of the comparison electrode with the same frequency allocation as the reference. For the SSD-CI subjects, the spiral-ganglion map formed the basis of the translation between matched acoustic frequency and the cochlear place of stimulation for each electrode contact (i.e., the electrode insertion angle; Fig. 2E,F). Mismatch was calculated by comparing the insertion angle associated with the matched acoustic frequency (according to the spiral-ganglion map) to the insertion angle associated with the reference-electrode CF. Zero mismatch meant that the relative place of stimulation in the two ears was aligned with the CI frequency allocation. For BI-CI subjects, this meant that two electrodes tuned to the same frequency stimulated the same cochlear places in the two ears. For SSD-CI subjects, this meant that a given electrode stimulated the cochlear place associated with the clinically

allocated frequency of the electrode. In both cases, zero mismatch meant that an acoustic tone at the allocated frequency of the electrode would stimulate the same place in both ears.

The pairwise relationships among the three methods of mismatch are plotted in Figure 6. The BI-CI results are shown in the top row (Fig. 6A–C), and the SSD-CI results are shown in the bottom row (Fig. 6D–F), with each symbol/color combination in a given row representing a different subject and with each data point representing one individual electrode. Data are plotted for only those reference electrodes where data were available for all three methods. The shaded squares near the center of each diagram represent the mismatch range of binaural tolerance, approximately ±75°, which is roughly equivalent to ±3 mm on the Greenwood scale over which binaural sensitivity is relatively insensitive to mismatch for BI-CI subjects (Kan et al., 2013,
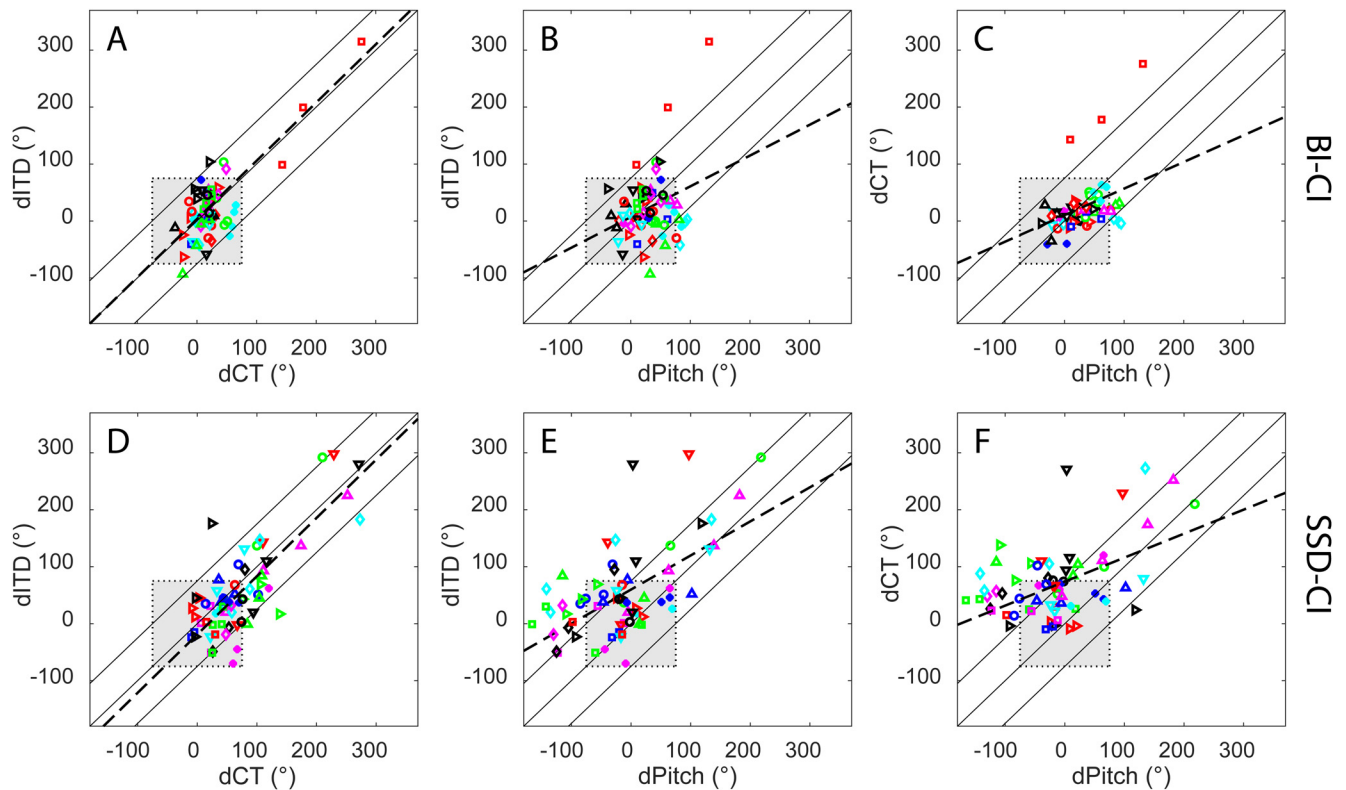
Figure 6. Pairwise comparisons of the three estimates of the magnitude of interaural place mismatch for individual electrodes for ***A–C***, the BI-CI subjects, and ***D–F***, the SSD-CI subjects, with each color/symbol combination representing a different subject. The three diagonal lines indicate 1:1 correspondence (±75°) where two mismatch estimates are not different. The gray shaded box indicates the ±75° mismatch range (equivalent to 3 mm on the Greenwood scale) over which binaural sensitivity is estimated to be tolerant to mismatch (Kan et al., 2013). The dashed lines represent linear fits from a regression analysis.

2015). Points falling within this square indicate electrodes for which both methods show an interaural place mismatch that is smaller than this tolerance range. The center solid diagonal line in each diagram represents a 1:1 correspondence (i.e., the two methods in question give the same estimate of interaural mismatch), whereas the upper and lower solid lines indicate the ±75° range around the center diagonal line. The dashed lines represent linear fits from the regression analysis.

For the BI-CI subjects (Fig. 6A–C), the estimated interaural mismatch was outside the 75° tolerance range for very few of the electrodes tested (ITD, 10%; Pitch, 12%; CT, 5%). Notably, only one subject had any electrodes with >75° mismatch based on CT scan estimates (BI9, red squares). For the SSD-CI subjects (Fig. 6D–F), mismatch estimates fell outside of the 75° tolerance range for about one-third of the electrodes tested (ITD, 25%; Pitch, 36%; CT, 36%). Comprehensive analyses are described below that examine the tonotopic relationships among the three methods. It was nevertheless instructive to carry out an initial set of pairwise analyses to get a sense of the relationships among the three methods. Bonferroni-corrected linear mixed-model regression analyses were conducted for each of the three pairwise comparisons of mismatch for the two subject groups (criterion p value for six comparisons = 0.0083). In each analysis, the estimate on the vertical axis was treated as the outcome variable, the estimate on the horizontal axis as a fixed effect, and subject as a random effect. To provide a sense of the strength of the pairwise relationships, estimated marginal R^2 values associated with adding to the model the variable represented on the horizontal axis are reported. These values were derived using the r2 function from the sjstats library for R.

The left column of Figure 6 shows the relationship between dITD and dCT. For the BI-CI subjects (Fig. 6A), dITD and dCT appeared related [χ^2 (1) = 48.3, $p < 0.0001$, $R^2 = 0.61$] and there was a slope not significantly different from unity (B = 1.02, $p = 0.85$, dashed line). However, this may largely reflect the contribution of one subject with large mismatch (BI9, red squares). With this subject excluded from the analysis, the relationship remained significant, albeit weaker [χ^2 (1) = 9.38, $p = 0.002$, $R^2 = 0.16$] with a regression slope that was shallower but still not significantly different from unity (B = 0.72, $p = 0.23$, linear fit not shown). For the SSD-CI subjects (Fig. 6D), dITD and dCT were strongly related [χ^2 (1) = 64.4, $p < 0.0001$, $R^2 = 0.64$], and these two mismatch estimates were nearly equal, with a regression slope that was not significantly different from unity (B = 1.02, $p = 0.81$, dashed line). Most of the points in Figure 6D are near the 1:1 line with few points falling outside the ±75° diagonal region.

The middle and right columns of Figure 6 show the relationships between dPitch and the other two methods. For the BI-CI subjects, there was a weak but significant relationship between dPitch and dITD [χ^2 (1) = 7.94, $p = 0.005$, $R^2 = 0.10$; Fig. 6B, dashed line], but this relationship became nonsignificant when the outlier subject was excluded from the analysis ($p = 0.61$). There was also a weak but significant relationship between dPitch and dCT [χ^2 (1) = 20.7, $p < 0.0001$, $R^2 = 0.12$; Fig. 6C, dashed line]. This relationship remained significant even with the outlier subject excluded from the analysis [χ^2 (1) = 8.85, $p = 0.003$, $R^2 = 0.13$], but with a regression slope that was much shallower than unity (B = 0.08, $p < 0.0001$, linear fit not shown).

For the SSD-CI subjects, there were also significant relationships between dPitch and dITD [χ^2 (1) = 31.0, $p < 0.0001$, $R^2 = $
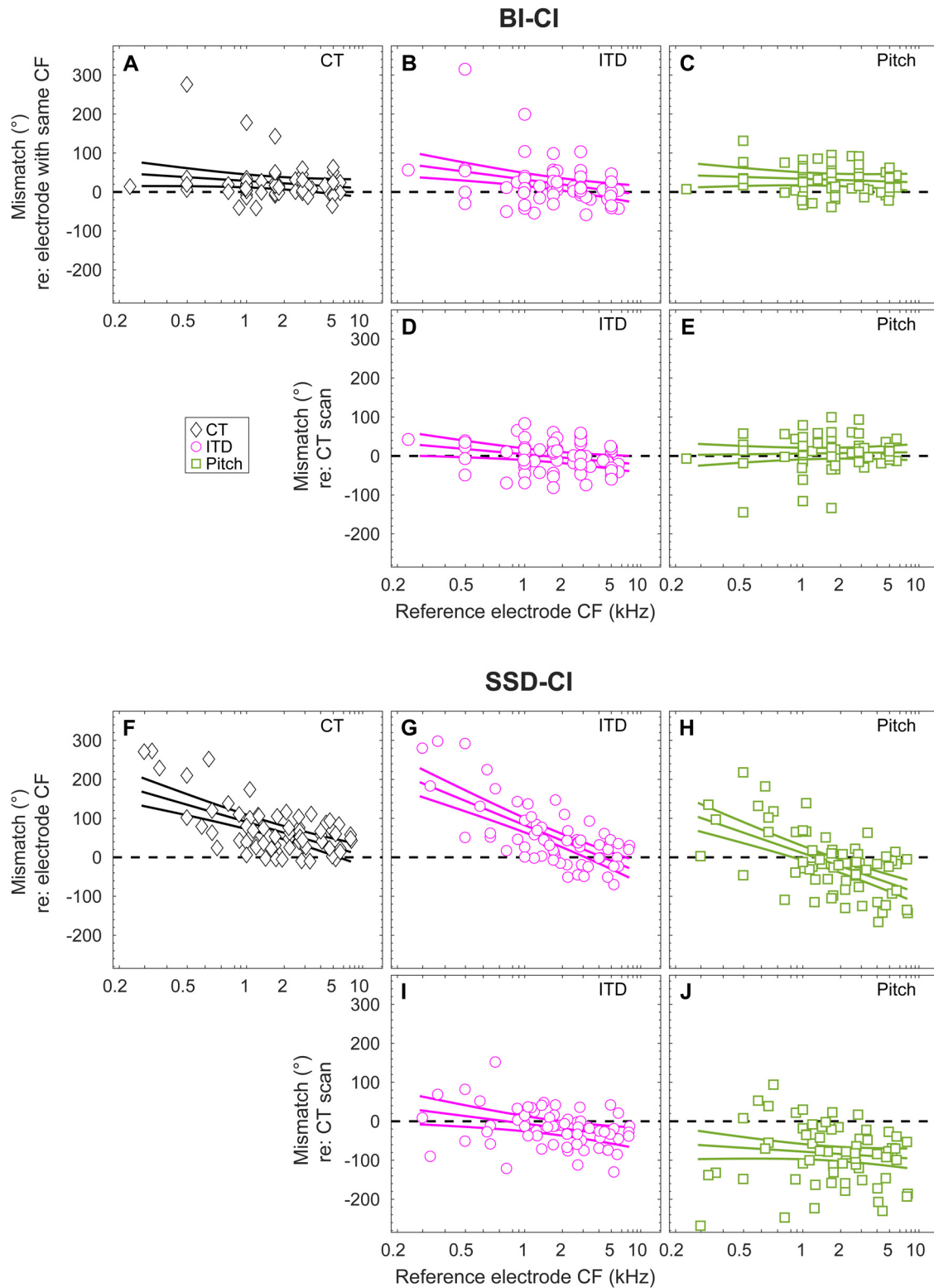
Figure 7. Tonotopic dependence of interaural place mismatch for **A–E**, BI-CI subjects, and **F–J**, SSD-CI subjects. The first and third rows reference the mismatch to the clinical map, based on **A–C**, the insertion angle associated with the number-matched electrode for BI-CI subjects, or **F–H**, the insertion angle associated with the reference electrode CF for SSD-CI subjects. The second and fourth rows (**D**, **E** and **I**, **J**) reference the mismatch to the CT estimate of electrode position. Points represent mismatch measurements for individual electrodes; fitted curves represent estimates of the group average and 95% confidence interval. Horizontal dashed lines indicate zero mismatch.

0.38; Fig. 6E] and between dPitch and dCT [χ^2 (1) = 17.9, $p <$ 0.0001, R^2 = 0.27; Fig. 6F]. Despite these significant relationships, many of the points fell outside the region indicated by the upper and lower diagonal lines in Figure 6, E and F, indicating that

dPitch differed from dITD or dCT by >75°. Furthermore, the regression slopes involving dPitch were significantly smaller than unity (dCT versus dPitch: B = 0.42, $p <$ 0.0001, Fig. 6E, dashed line; dITD versus dPitch: B = 0.60, $p <$ 0.0001, Fig. 6F, dashed

line). Thus, considering the scatter in the data and the shallow slopes for each relationship, dPitch differed substantially from these other estimates despite the significant correlations.

In summary, Figure 6, A–C, shows the significant relationships among the three mismatch methods for the BI-CI subjects largely depended on the one subject (BI9) for whom CT scans showed a large mismatch. However, even with this subject excluded from the analysis, there was still a weak but significant relationship between dITD and dCT with a slope not significantly different from unity (Fig. 6A). There was also a weak but significant relationship between dPitch and dCT, but with a shallow slope suggesting a lack of 1:1 alignment (Fig. 6C). For the SSD-CI subjects, there was a strong significant relationship between dITD and dCT, with a slope near unity (Fig. 6D). There were also significant relationships between dPitch and dITD (Fig. 6E), and dPitch and dCT (Fig. 6F); however, the slopes of these relationships were shallow, and there was substantial scatter in the data, suggesting that dPitch did not align closely with the other two methods.

Tonotopic dependence of interaural frequency mismatch

Figure 6 does not account for how the relationship between mismatch estimates might change as a function of intracochlear location. For example, for many SSD-CI subjects (Fig. 5B), dPitch (green squares) had a shallower slope with respect to the reference-electrode CF than the slope of dCT (white diamonds) or the slope of dITD (magenta circles). This suggests that the relationship between the mismatch estimates was dependent on the cochlear region being stimulated.

The three estimates of interaural frequency mismatch are plotted as a function of location along CI array for the BI-CI subjects (Fig. 7A–E) and for the SSD-CI subjects (Fig. 7F–J). A primary question posed in this study was whether the pitch and ITD methods of estimating electrode position were more closely aligned with the frequencies allocated to each electrode in the sound processor (indicating plasticity in the percept that aligned with mismatch) or with the CT scan estimates (indicating a lack of plasticity to any existing frequency mismatch). To pose this question, mismatch was defined in two different ways. The first (Fig. 7A–C) and third rows (Fig. 7F–H) plot the estimated mismatch with respect to the reference-electrode CF. Here, mismatch estimates near zero indicated close alignment with the frequency allocation of the CI sound processor. The second (Fig. 7D,E) and fourth rows (Fig. 7I,J) plot the estimated mismatch with respect to the insertion angle estimates from the CT scan. Here, mismatch estimates near zero indicate close alignment with physical electrode location. The three solid curves in each diagram of Figure 7 represent the estimated group mean and 95% confidence interval of the mismatch for a given cochlear location. Electrode locations for which the 95% confidence interval does not include zero indicate a significant group-average mismatch.

For the BI-CI subjects, all three estimates of interaural mismatch gave similar average results (Fig. 7A–C). A linear mixed-model regression analyses with two fixed-effect factors (interaural-matching method and reference-electrode CF) found no significant main effect of the interaural-matching method [χ^2 (2) = 2.67, p = 0.26], or interaction between these two factors [χ^2 (2) = 3.83, p = 0.15]. There was a significant effect of reference-electrode CF [χ^2 (1) = 9.73, p = 0.002]; Figure 7A shows there was a small average interaural mismatch that ranged from 54° for a CF of 250 Hz to 10° for a CF of 8000 Hz. The effect of reference-electrode CF remained significant even with the outlier removed

from the analysis [χ^2 (1) = 5.91, p = 0.015, 37° at 250 Hz, 9° at 8000 Hz, linear fit not shown]. In other words, there was, on average, a small but significant mismatch for the apical (low-frequency) portion of the array. When calculated relative to the CT estimates of electrode position, neither dPitch nor dITD was significantly different from zero (confidence intervals in Fig. 7D–E include zero). In summary, this means that on average across the subjects, none of the three methods were different from one another.

For the SSD-CI subjects, the mismatch estimates clearly differed among methods (Fig. 7F–H). This observation was supported by a linear mixed-model regression analyses conducted on the mismatch estimates with respect to each reference-electrode CF. There were significant main effects of CF [χ^2 (1) = 112, p < 0.0001] and method [χ^2 (2) = 54.7, p < 0.0001], but no significant interaction between the two variables [χ^2 (2) = 3.45, p = 0.18]. For all three methods, there was greater positive mismatch for the apical compared with the basal portion of the array. Relative to the reference-electrode CF, dCT was significantly greater than zero across the length of the array (Fig. 7F), indicating that the electrode location was shifted basally to the reference-electrode CF, as expected. Likewise, dITD (Fig. 7G) was significantly greater than zero across the apical and middle portions of the array, becoming nonsignificant for the basal portion. In contrast, the direction of dPitch varied across the electrode array (Fig. 7H). At low frequencies, there was mismatch in the expected positive (basal) direction, whereas at high frequencies there was mismatch in the unexpected negative (apical) direction.

Relative to the CT scan, dPitch (Fig. 7J) was significantly negative for the full frequency range, meaning that the pitch associated with a given electrode was lower than expected given the electrode position. In contrast, dITD (Fig. 7I) was not significantly different from zero for most of the array, meaning that binaural sensitivity was best for an acoustic frequency at the electrode position indicated by the CT scan, except at the very basal end of the array, where dITD was slightly negative.

In summary, there was on average very little mismatch for the BI-CI subjects and no discernable difference among dITD, dPitch, and dCT (Fig. 7A–C). In contrast, all three methods showed considerable group-average mismatch for the SSD-CI subjects, which varied across the length of the electrode array (Fig. 7F–H). The pitch estimates aligned with neither the reference-electrode CF (Fig. 7H) nor the CT-estimated electrode position (Fig. 7J). The ITD and CT estimates produced similar patterns of mismatch; relative to the reference-electrode CF (Fig. 7F–G), both methods showed a large average mismatch for the apical portion of the array that decreased to near zero for the basal portion. When referenced to the CT estimate of electrode position, the ITD method showed no significant mismatch except for a small negative mismatch for the basal portion of the array (Fig. 7I).

Discussion

Although the auditory system exhibits central plasticity following peripheral changes stemming from hearing loss and CIs (Fallon et al., 2009), it is unclear if the adult human binaural system is sufficiently plastic to overcome interaural place mismatch (Kan et al., 2013, 2015; Reiss et al., 2014, 2015; Aronoff et al., 2016, 2019). Other aspects of spatial auditory perception might be more readily rectified by plasticity. For example, normal-hearing adult humans (Shinn-Cunningham et al., 1998a,b; Keating

et al., 2016) and juvenile ferrets (Keating et al., 2013) demonstrate behavioral adaptation to artificial changes to the mapping between ITD or ILD and spatial location, whereas the optic tectum of developing owls (Mogdans and Knudsen, 1992; Linkenhoker and Knudsen, 2002) and the juvenile and adult ferret cortex (Keating et al., 2013, 2016) exhibit neurophysiological adaptation to similar changes.

This study asked if binaural or place-pitch perception undergo plasticity to resolve interaural place mismatch. By comparing binaural tuning to radiographic images of physical electrode position, these results extend previous findings of frequency-tuned binaural sensitivity for BI-CI (Hu and Dietz, 2015; Kan et al., 2015), SSD-CI (Bernstein et al., 2018; Francart et al., 2018; Dirks et al., 2020), and bimodal-CI subjects (Francart et al., 2011, 2014). For postlingually deafened adults, adaptation for CI speech understanding is thought to saturate by 6 months for BI-CIs (Reeder et al., 2014) and 3 months for SSD-CIs (Buss et al., 2018). All subjects in the current study had >6 months of CI experience, with most subjects having >1 year. Plasticity over this period of device use was inferred from comparisons among the mismatch estimation methods; a behavioral estimate aligned with a CT estimate of mismatch was interpreted as lack of plasticity, and a shift toward the frequency allocation of the electrode in the CI sound processor map was interpreted as an indication of adaptation (Reiss et al., 2014).

Overall, the results showed little interaural place mismatch for BI-CI subjects, apart from a single outlier. In contrast, there was systematic mismatch for SSD-CI subjects, with many electrodes showing >75° of mismatch, especially toward the apex. This result supports our hypothesis that BI-CI users would show less mismatch because of more symmetric peripheral input. This group difference reflects the anatomic difference underlying mismatch (Figs. 3, 4). For BI-CI users, interaural place mismatch reflects relative placement of the arrays in the two ears. For SSD-CI users, interaural place mismatch reflects the relationship between electrode placement and the acoustic tonotopy of the cochlea. Although both groups showed similar tonotopic mismatch (electrode array versus the acoustic frequency map; Fig. 4A,B) this only affected interaural place mismatch for SSD-CI users (Fig. 4C).

Because of the lack of BI-CI mismatch, little can be said about the question of plasticity for binaural or pitch perception for these individuals. Hu and Dietz (2015) also investigated this question for BI-CI subjects. They found that electrophysiological and psychophysical estimates of mismatch for binaural processing were mutually consistent but differed from pitch-based estimates that showed little mismatch. This could be interpreted as indicating plasticity for pitch but not for binaural processing. However, the small sample ($N = 7$, one electrode per subject) precluded statistical assessment of these relationships, and without electrode-position imaging, these data only indirectly addressed the question of plasticity. Although the current study included a larger sample and CT scans, the BI-CI subjects lacked sufficient interaural place mismatch to assess plasticity.

In contrast to the BI-CI subjects, the frequently occurring mismatch for the SSD-CI subjects allowed for an assessment of plasticity to mismatch. In line with our hypothesis, the SSD-CI data suggested that plasticity does not overcome interaural place mismatch for binaural tuning. ITD discrimination and CT scans gave similar estimates of mismatch (nearly all electrodes fell within the ±75° diagonal; Fig. 6D). Furthermore, both methods

showed similar tonotopic dependence, with large mismatch toward the apex decreasing to zero toward the base (Fig. 7F,G). This trend differs from other radiographic studies of acoustic-electric mismatch for monaural CI users that show little tonotopic dependence (Landsberger et al., 2015; Canfarotta et al., 2020), except for a slight tendency for more mismatch near the apex. Note that these previous studies based the estimates on the standard frequency allocation of the manufacturer. In the current study, we were specifically interested in comparing mismatch estimates relative to the frequency allocation in each subject's everyday sound processor; this is important because several subjects had deactivated electrodes or other changes that altered the frequency-to-electrode allocation. The frequencies allocated to the most basal active electrodes were sometimes shifted upward from the manufacturer default (Fig. 3B), likely explaining some of the discrepancy with previous studies.

We also hypothesized that because pitch comparisons involve central comparison of two sequential sounds (one in each ear), and no binaural brainstem processing, this percept would be more likely to exhibit plasticity to interaural place mismatch. Although there was little correspondence between SSD-CI interaural pitch matches and CT-scan based estimates of cochlear position (Figs. 6F, 7J), suggesting the possibility of plasticity, pitch matches did not align with the sound processor frequency allocation (Fig. 7H). The pitch estimates were consistently lower than even the reference-electrode CF in the basal half of the array (Fig. 7H), which is inconsistent with a hypothesized shift in place pitch toward the reference-electrode CF.

The literature is mixed regarding the question of CI pitch plasticity. Some studies have shown pitch perception to shift toward the sound-processor frequency allocation (Reiss et al., 2014; Hu and Dietz, 2015; Tan et al., 2017), and others have not (Schatzer et al., 2014; Aronoff et al., 2016; Marozeau et al., 2020). One possible reason for the disparate results is that the procedures (Jensen et al., 2021) and stimuli (Adel et al., 2019) used have a large impact on the observed results, questioning whether these measurements reflect place of stimulation. In the current study, the unexpected tonotopic pattern of SSD-CI pitch-match estimates (positive at the apex, negative at the base; Fig. 7H) might reflect a procedural bias where the match gravitated toward the center of the available comparison-frequency range (Carlyon et al., 2010; Goupell et al., 2019).

Despite the clear relationship observed between ITD and CT-scan (but not pitch) estimates of SSD-CI mismatch, there were at least four study limitations that provide clear future directions. First, most of the BI-CI subjects had little interaural place mismatch (Figs. 3-7). Future work examining BI-CI subjects with larger mismatch would strengthen any assessment of binaural plasticity. Whereas the current sample had only one subject with large mismatch, Goupell et al. (2021) examined CT scans for 107 BI-CI subjects (including the 19 from the current study) and found that 13% of electrode pairs had a mismatch >75°.

Second, this study was performed acutely. Many subjects had used their CI(s) for multiple years, but some for as little as 6 months (Tables 1, 2). Any adaptation these subjects were experiencing might have been incomplete, particularly for binaural processing where performance can continue to improve for up to 4 years (Eapen et al., 2009). A longitudinal study of ITD and pitch changes over years could address this limitation.

Third, it is unclear if the pitch results reflect plasticity or procedural biases, which are common and often large for CI subjects (Carlyon et al., 2010; Goupell et al., 2019; Jensen et al., 2021). These studies proposed various checks for systematic biases.

Nearly all the individual pitch-match estimates here passed one of these checks (independence from the adaptive-track starting point, Carlyon et al., 2010), yet Jensen et al. (2021) found that adaptive methods can pass this check and still be susceptible to other biases. Although Jensen et al. (2021) found the ranking procedure used here to be largely immune to three different kinds of systematic bias for BI-CI subjects, that study did not include SSD-CI subjects, the group that showed deviation between pitch and CT matches in the current study.

Fourth, this study did not estimate possible local auditory-nerve degeneration (Long et al., 2014). CT imaging assesses electrode placement but not the number and health of the spiral ganglion cells that are electrically stimulated. An assessment of neural responses and inferred survival, for example, using electrically evoked compound action potential measurements, might account for some of the deviation between the CT and perceptual methods (Bierer, 2010; Long et al., 2014; DeVries et al., 2016).

In closing, we note that this study serves a practical purpose informing clinical practice. Because SSD-CI binaural sensitivity appears not to adapt to interaural place mismatch, maximizing binaural performance will likely require intervention by adjusting the CI sound processor frequency allocation. This could also be the case for BI-CI users with large mismatches. Sheffield et al. (2020) found that frequencies <1200 Hz can be discarded to match CI-ear and acoustic-ear cochlear places of stimulation without reducing the speech-in-noise benefit provided by a SSD-CI. CT-scan estimates of interaural place mismatch showed relatively close agreement with time-consuming ITD-based estimates (Figs. 6, 7). With the caveat that it involves a small but not insignificant radiation exposure, CT imaging may prove to be an effective clinical tool to measure interaural place mismatch, guiding the audiologist in frequency mapping to optimize binaural processing without requiring extensive psychophysical testing.

References

Adel Y, Nagel S, Weissgerber T, Baumann U, Macherey O (2019) Pitch matching in cochlear implant users with single-sided deafness: effects of electrode position and acoustic stimulus type. Front Neurosci 13:1119.

Aronoff JM, Padilla M, Stelmach J, Landsberger DM (2016) Clinically paired electrodes are often not perceived as pitch matched. Trends Hear 20:233121651666830.

Aronoff JM, Staisloff HE, Kirchner A, Lee DH, Stelmach J (2019) Pitch matching adapts even for bilateral cochlear implant users with relatively small initial pitch differences across the ears. J Assoc Res Otolaryngol 20:595–603.

Bernstein JGW, Oxenham AJ (2003) Pitch discrimination of diotic and dichotic tone complexes: harmonic resolvability or harmonic number? J Acoust Soc Am 113:3323–3334.

Bernstein JGW, Goupell MJ, Schuchman GI, Rivera AL, Brungart DS (2016) Having two ears facilitates the perceptual separation of concurrent talkers for bilateral and single-sided deaf cochlear implantees. Ear Hear 37:289–302.

Bernstein JGW, Schuchman GI, Rivera AL (2017) Head shadow and binaural squelch for unilaterally deaf cochlear implantees. Otol Neurotol 38:e195–e202.

Bernstein JGW, Stakhovskaya OA, Schuchman GI, Jensen KK, Goupell MJ (2018) Interaural time-difference discrimination as a measure of place of stimulation for cochlear-implant users with single-sided deafness. Trends Hear 22:2331216518765514.

Bierer JA (2010) Probing the electrode-neuron interface with focused cochlear implant stimulation. Trends Amplif 14:84–95.

Blanks DA, Roberts JM, Buss E, Hall JW, Fitzpatrick DC (2007) Neural and behavioral sensitivity to interaural time differences using amplitude modulated tones with mismatched carrier frequencies. J Assoc Res Otolaryngol 8:393–408.

Buss E, Dillon MT, Rooth MA, King ER, Deres EJ, Buchman CA, Pillsbury HC, Brown KD (2018) Effects of cochlear implantation on binaural hearing in adults with unilateral hearing loss. Trends Hear 22:2331216518771173.

Canfarotta MW, Dillon MT, Buss E, Pillsbury HC, Brown KD, O'Connell BP (2020) Frequency-to-place mismatch: characterizing variability and the influence on speech perception outcomes in cochlear implant recipients. Ear Hear 41:1349–1361.

Carlyon RP, Macherey O, Frijns JHM, Axon PR, Kalkman RK, Boyle P, Baguley DM, Briggs J, Deeks JM, Briaire JJ, Barreau X, Dauman R (2010) Pitch comparisons between electrical stimulation of a cochlear implant and acoustic stimuli presented to a normal-hearing contralateral ear. J Assoc Res Otolaryngol 11:625–640.

Chung Y, Hancock KE, Delgutte B (2016) Neural coding of interaural time differences with bilateral cochlear implants in unanesthetized rabbits. J Neurosci 36:5520–5531.

Churchill TH, Kan A, Goupell MJ, Litovsky RY (2014) Spatial hearing benefits demonstrated with presentation of acoustic temporal fine structure cues in bilateral cochlear implant listeners. J Acoust Soc Am 136:1246–1256.

Cootes TF, Taylor CJ, Cooper DH, Graham J (1995) Active shape models—their training and application. Comput Vis Image Underst 61:38–59.

Cosentino S, Carlyon RP, Deeks JM, Parkinson W, Bierer JA (2016) Rate discrimination, gap detection and ranking of temporal pitch in cochlear implant users. J Assoc Res Otolaryngol 17:371–382.

DeVries L, Scheperle R, Bierer JA (2016) Assessing the electrode-neuron interface with the electrically evoked compound action potential, electrode position, and behavioral thresholds. J Assoc Res Otolaryngol 17:237–252.

Dirks CE, Nelson PB, Winn MB, Oxenham AJ (2020) Sensitivity to binaural temporal-envelope beats with single-sided deafness and a cochlear implant as a measure of tonotopic match (L). J Acoust Soc Am 147:3626–3630.

Eapen RJ, Buss E, Adunka MC, Pillsbury HC 3rd, Buchman CA (2009) Hearing-in-noise benefits after bilateral simultaneous cochlear implantation continue to improve 4 years after implantation. Otol Neurotol 30:153–159.

Fallon JB, Irvine DR, Shepherd RK (2009) Neural prostheses and brain plasticity. J Neural Eng 6:065008.

Fitzgerald MB, Kan A, Goupell MJ (2015) Bilateral loudness balancing and distorted spatial perception in recipients of bilateral cochlear implants. Ear Hear 36:e225–e236.

Francart T, Lenssen A, Wouters J (2011) Sensitivity of bimodal listeners to interaural time differences with modulated single- and multiple-channel stimuli. Audiol Neurootol 16:82–92.

Francart T, Lenssen A, Wouters J (2014) Modulation enhancement in the electrical signal improves perception of interaural time differences with bimodal stimulation. J Assoc Res Otolaryngol 15:633–647.

Francart T, Wiebe K, Wesarg T (2018) Interaural time difference perception with a cochlear implant and a normal ear. J Assoc Res Otolaryngol 19:703–715.

Gabor D (1947) Acoustical quanta and the theory of hearing. Nature 159:591–594.

Goodman TR, Mustafa A, Rowe E (2019) Pediatric CT radiation exposure: where we were, and where we are now. Pediatr Radiol 49:469–478.

Goupell MJ, Majdak P, Laback B (2010) Median-plane sound localization as a function of the number of spectral channels using a channel vocoder. J Acoust Soc Am 127:990–1001.

Goupell MJ, Stoelb C, Kan A, Litovsky RY (2013) Effect of mismatched place-of-stimulation on the salience of binaural cues in conditions that simulate bilateral cochlear-implant listening. J Acoust Soc Am 133:2272–2287.

Goupell MJ, Stakhovskaya OA, Bernstein JGW (2018) Contralateral interference caused by binaurally presented competing speech in adult bilateral cochlear-implant users. Ear Hear 39:110–123.

Goupell MJ, Cosentino S, Stakhovskaya OA, Bernstein JGW (2019) Interaural pitch-discrimination range effects for bilateral and single-sided-deafness cochlear-implant users. J Assoc Res Otolaryngol 20:187–203.

Goupell MJ, Noble JH, Phatak SA, Kolberg E, Cleary M, Stakhovskaya OA, Jensen KK, Hoa M, Kim HJ, Bernstein JGW (2021) Computed-tomography estimates of interaural mismatch in insertion depth and scalar location in bilateral cochlear-implant users. medRxiv. Advance online publication. Retrieved November 1, 2021.

Greenwood DD (1990) A cochlear frequency-position function for several species—29 years later. J Acoust Soc Am 87:2592–2605.

Hancock KE, Chung Y, Delgutte B (2013) Congenital and prolonged adult-onset deafness cause distinct degradations in neural ITD coding with bilateral cochlear implants. J Assoc Res Otolaryngol 14:393–411.

Hu H, Dietz M (2015) Comparison of interaural electrode pairing methods for bilateral cochlear implants. Trends Hear 19:233121651561714.

Jensen KK, Cosentino S, Bernstein JGW, Stakhovskaya OA, Goupell MJ (2021) A comparison of place-pitch-based interaural electrode matching methods for bilateral cochlear-implant users. Trends Hear 25:2331216521997324.

Kan A, Litovsky RY (2015) Binaural hearing with electrical stimulation. Hear Res 322:127–137.

Kan A, Stoelb C, Litovsky RY, Goupell MJ (2013) Effect of mismatched place-of-stimulation on binaural fusion and lateralization in bilateral cochlear-implant users. J Acoust Soc Am 134:2923–2936.

Kan A, Litovsky RY, Goupell MJ (2015) Effects of interaural pitch matching and auditory image centering on binaural sensitivity in cochlear implant users. Ear Hear 36:e62–e68.

Keating P, Dahmen JC, King AJ (2013) Context-specific reweighting of auditory spatial cues following altered experience during development. Curr Biol 23:1291–1299.

Keating P, Rosenior-Patten O, Dahmen JC, Bell O, King AJ (2016) Behavioral training promotes multiple adaptive processes following acute hearing loss. Elife 5:e12264.

Landsberger DM, Svrakic M, Roland JT, Svirsky M (2015) The relationship between insertion angles, default frequency allocations, and spiral ganglion place pitch in cochlear implants. Ear Hear 36:207–213.

Linkenhoker BA, Knudsen EI (2002) Incremental training increases the plasticity of the auditory space map in adult barn owls. Nature 419:293–296.

Litovsky RY, Goupell MJ, Godar S, Grieco-Calub T, Jones GL, Garadat SN, Agrawal S, Kan A, Todd A, Hess C, Misurelli S (2012) Studies on bilateral cochlear implants at the University of Wisconsin's Binaural Hearing and Speech Laboratory. J Am Acad Audiol 23:476–494.

Long CJ, Nimmo-Smith I, Baguley DM, O'Driscoll M, Ramsden R, Otto SR, Axon PR, Carlyon RP (2005) Optimizing the clinical fit of auditory brain stem implants. Ear Hear 26:251–262.

Long CJ, Holden TA, McClelland GH, Parkinson WS, Shelton C, Kelsall DC, Smith ZM (2014) Examining the electro-neural interface of cochlear implant users using psychophysics, CT scans, and speech understanding. J Assoc Res Otolaryngol 15:293–304.

Maes F, Collignon A, Vandermeulen D, Marchal G, Suetens P (1997) Multimodality image registration by maximization of mutual information. IEEE Trans Med Imaging 16:187–198.

Marozeau J, Gnansia D, Ardoint M, Poncet-Wallet C, Lazard DS (2020) The sound sensation of a pure tone in cochlear implant recipients with single-sided deafness. PLoS One 15:e0235504.

Mettler FA, Mahesh M, Bhargavan-Chatfield M, Chambers CE, Elee JG, Frush DP, Miller DL, Royal HD, Milano MT, Spelic DC, Ansari AJ, Bolch WE, Guebert GM, Sherrier RH, Smith JM, Vetter RJ (2020) Patient exposure from radiologic and nuclear medicine procedures in the United States: procedure volume and effective dose for the period 2006–2016. Radiology 295:418–427.

Mogdans J, Knudsen EI (1992) Adaptive adjustment of unit tuning to sound localization cues in response to monaural occlusion in developing owl optic tectum. J Neurosci 12:3473–3484.

Noble JH, Labadie RF, Majdani O, Dawant BM (2011) Automatic segmentation of intra-cochlear anatomy in conventional CT. IEEE Trans Biomed Eng 58:2625–2632.

Peters BR, Wyss J, Manrique M (2010) Worldwide trends in bilateral cochlear implantation. Laryngoscope 120:S17–S44.

Poon BB, Eddington DK, Noel V, Colburn HS (2009) Sensitivity to interaural time difference with bilateral cochlear implants: development over time and effect of interaural electrode spacing. J Acoust Soc Am 126:806–815.

Reda FA, McRackan TR, Labadie RF, Dawant BM, Noble JH (2014) Automatic segmentation of intra-cochlear anatomy in post-implantation CT of unilateral cochlear implant recipients. Med Image Anal 18:605–615.

Reeder RM, Firszt JB, Holden LK, Strube MJ (2014) A longitudinal study in adults with sequential bilateral cochlear implants: time course for individual ear and bilateral performance. J Speech Lang Hear Res 57:1108–1126.

Reiss LA, Turner CW, Erenberg SR, Gantz BJ (2007) Changes in pitch with a cochlear implant over time. J Assoc Res Otolaryngol 8:241–257.

Reiss LA, Turner CW, Karsten SA, Gantz BJ (2014) Plasticity in human pitch perception induced by tonotopically mismatched electro-acoustic stimulation. Neuroscience 256:43–52.

Reiss LA, Ito RA, Eggleston JL, Liao S, Becker JJ, Lakin CE, Warren FM, McMenomey SO (2015) Pitch adaptation patterns in bimodal cochlear implant users: over time and after experience. Ear Hear 36:e23–e34.

Robertson D, Irvine DR (1989) Plasticity of frequency organization in auditory cortex of guinea pigs with partial unilateral deafness. J Comp Neurol 282:456–471.

Schatzer R, Vermeire K, Visser D, Krenmayr A, Kals M, Voormolen M, Van de Heyning P, Zierhofer C (2014) Electric-acoustic pitch comparisons in single-sided-deaf cochlear implant users: frequency-place functions and rate pitch. Hear Res 309:26–35.

Schuman TA, Noble JH, Wright CG, Wanna GB, Dawant B, Labadie RF (2010) Anatomic verification of a novel method for precise intrascalar localization of cochlear implant electrodes in adult temporal bones using clinically available computed tomography. Laryngoscope 120:2277–2283.

Sheffield SW, Goupell MJ, Spencer NJ, Stakhovskaya OA, Bernstein JGW (2020) Binaural optimization of cochlear implants: discarding frequency content without sacrificing head-shadow benefit. Ear Hear 41:576–590.

Shinn-Cunningham BG, Durlach NI, Held RM (1998a) Adapting to super-normal auditory localization cues. I. Bias and resolution. J Acoust Soc Am 103:3656–3666.

Shinn-Cunningham BG, Durlach NI, Held RM (1998b) Adapting to super-normal auditory localization cues. II. Constraints on adaptation of mean response. J Acoust Soc Am 103:3667–3676.

Stakhovskaya O, Sridhar D, Bonham BH, Leake PA (2007) Frequency map for the human cochlear spiral ganglion: implications for cochlear implants. J Assoc Res Otolaryngol 8:220–233.

Suneel D, Staisloff H, Shayman CS, Stelmach J, Aronoff JM (2017) Localization performance correlates with binaural fusion for interaurally mismatched vocoded speech. J Acoust Soc Am 142:EL276.

Svirsky MA, Silveira A, Neuburger H, Teoh S-W, Suárez H (2004) Long-term auditory adaptation to a modified peripheral frequency map. Acta Otolaryngol 124:381–386.

Tan C-T, Martin B, Svirsky MA (2017) Pitch matching between electrical stimulation of a cochlear implant and acoustic stimuli presented to a contralateral ear with residual hearing. J Am Acad Audiol 28:187–199.

Van Wanrooij MM, Van Opstal AJ (2005) Relearning sound localization with a new ear. J Neurosci 25:5413–5424.

Verbist BM, Skinner MW, Cohen LT, Leake PA, James C, Boëx C, Holden TA, Finley CC, Roland PS, Roland JT, Haller M, Patrick JF, Jolly CN, Faltys MA, Briaire JJ, Frijns JHM (2010) Consensus panel on a cochlear coordinate system applicable in histologic, physiologic, and radiologic studies of the human cochlea. Otol Neurotol 31:722–730.

Wall BF (2009) Ionising radiation exposure of the population of the United States: NCRP Report No. 160. Radiat Prot Dosimetry 136:136–138.

Wang J, Noble JH, Dawant BM (2019) Metal artifact reduction for the segmentation of the intra cochlear anatomy in CT images of the ear with 3D-conditional GANs. Med Image Anal 58:101553.

Wess JM, Brungart DS, Bernstein JGW (2017) The effect of interaural mismatches on contralateral unmasking with single-sided vocoders. Ear Hear 38:374–386.

Yin TCT, Smith PH, Joris PX (2019) Neural mechanisms of binaural processing in the auditory brainstem. Compr Physiol 9:1503–1575.

Zhao Y, Chakravorti S, Labadie RF, Dawant BM, Noble JH (2019) Automatic graph-based method for localization of cochlear implant electrode arrays in clinical CT with sub-voxel accuracy. Med Image Anal 52:1–12.

Zirn S, Arndt S, Aschendorff A, Wesarg T (2015) Interaural stimulation timing in single sided deaf cochlear implant users. Hear Res 328:148–156.

Zwislocki JJ, Relkin EM (2001) On a psychophysical transformed-rule up and down method converging on a 75% level of correct responses. Proc Natl Acad Sci U S A 98:4811–4814.